Master's Thesis

Master's Programme in Particle Physics and Astrophysical Sciences

Theoretical Physics

Higgs mechanism and the correspondence of the Standard Model to LHC data

Joona Pankkonen

October 5, 2020

Supervisor(s): Kimmo Tuominen

Examiner(s): Kimmo Tuominen
Kari Rummukainen

University of Helsinki
Faculty of Science

PL 64 (Gustaf Hällströmin katu 2a)
00014 Helsingin yliopisto

HELSINGIN YLIOPISTO — HELSINGFORS UNIVERSITET — UNIVERSITY OF HELSINKI

Tiedekunta — Fakultet — Faculty	Koulutusohjelma — Utbildningsprogram — Degree programme
Faculty of Science	Master's Programme in Particle Physics and Astrophysical Sciences, Theoretical Physics

Tekijä — Författare — Author

Joona Pankkonen

Työn nimi — Arbetets titel — Title

Higgs mechanism and the correspondence of the Standard Model to LHC data

Työn laji — Arbetets art — Level	Aika — Datum — Month and year	Sivumäärä — Sidantal — Number of pages
Master's Thesis	October 5, 2020	56

Tiivistelmä — Referat — Abstract

The Standard Model is one of the accurate theories that we have. It has demonstrated its success by predictions and discoveries of new particles such as the existence of gauge bosons W and Z and heaviest quarks charm, bottom and top. After discovery of the Higgs boson in 2012 Standard Model became complete in sense that all elementary particles contained in it had been observed.

In this thesis I will cover the particle content and interactions of the Standard Model. Then I explain Higgs mechanism in detail. The main feature in Higgs mechanism is spontaneous symmetry breaking which is the key element for this mechanism to work. The Higgs mechanism gives rise to mass of the particles, especially gauge bosons.

Higgs boson was found at the Large Hadron Collider by CMS and ATLAS experiments. In the experiments, protons were collided with high energies (8-13 TeV). This leads to production of the Higgs boson by different production channels like gluon fusion (ggF), vector boson fusion (VBF) or the Higgsstrahlung. Since the lifetime of the Higgs boson is very short, it cannot be measured directly. In the CMS experiment Higgs boson was detected via channel $H \to ZZ \to 4\ell$ and via $H \to \gamma\gamma$.

In this thesis I examine the correspondence of the Standard Model to LHC data by using signal strengths of the production and decay channels by parametrizing the interactions of fermionic and bosonic production and decay channels. Data analysis carried by least squares method gave confidence level contours that describe how well the predictions of the Standard Model correspond to LHC data.

Avainsanat — Nyckelord — Keywords

Higgs boson, Higgs mechanism, Standard Model

Säilytyspaikka — Förvaringsställe — Where deposited

Muita tietoja — Övriga uppgifter — Additional information

Contents

Chapter 1

Introduction

The Standard Model (SM) is one of the accurate theories that we have. It has deepened our understanding in elementary particle physics and throughout the decades it has demonstrated its success by predictions and discoveries of new particles such as the existence of gauge bosons W and Z [1, 2]. The SM has also led to prediction of the existence of heaviest quarks charm [3], bottom [4] and top [5] which were found in 1974, 1977 and 1995 correspondingly. The most ambitious prediction was done by Peter Higgs when he predicted the existence of new scalar boson (Higgs boson) in 1964 that gives particles their mass [6]. After discovery of the Higgs boson in 2012 SM became complete in the sense that all elementary particles contained in it had been observed [7].

The Higgs mechanism revolves around the *spontaneous symmetry breaking* (SSB) which is the key element for this mechanism to work. The SSB describes the situation where a symmetric state ends up in asymmetric state and where the Lagrangian obeys symmetry, but the (lowest-energy) vacuum solutions do not exhibit the same symmetry. When the system ends up in one of the vacuum solutions, the symmetry breaks although the Lagrangian preserves the symmetry.

In the experiments at the Large Hadron Collider (LHC), protons are collided with each other at high energies (8-13 TeV) to produce Higgs boson via different production channels like gluon fusion (ggF), vector boson fusion (VBF) or the Higgsstrahlung. Since the lifetime of the Higgs boson is very short, it cannot be measured directly. At CERN the ATLAS and CMS experiments have confirmed the existence of the Higgs boson. In CMS experiment Higgs boson was detected via channel $H \to ZZ \to 4\ell$ [8] and via $H \to \gamma\gamma$ in the ATLAS experiment [9].

Despite the accurate predictions and success of the SM in particle physics, it still cannot anwser some questions. It is unable to explain dark matter, hierarchy problem or baryon asymmetry. Hence SM is not a complete theory. This means that we need to

extend SM somehow. One way to do this is to make extensions to Higgs sector as two-Higgs-doublet models, triplet models or Higgs portal models which includes interactions with dark matter. Also one may implement supersymmetry into SM which is minimal supersymmetric SM (MSSM).

In this thesis I give a general overview of the SM and go through Higgs mechanism and its principles thoroughly. The main focus of the thesis revolves around Higgs boson, its properties and how SM predictions correlate with the LHC data.

Chapter 2

The Standard Model

The Standard Model is a theory in particle physics which describes the fundamental forces in the universe. These forces are gravitational force, electromagnetic, strong and weak interaction. However the SM describes only three of these forces, not including gravity. All known elementary particles are classified as fermions or bosons. Furthermore the interactions can be described by different fields in the quantum field theory (QFT) where for each particle type there is a corresponding field i.e. electrons. The particles are interpreted as excitations in the fields.

Although the theoretical predictions and sufficient experimental confirmation of the particles such as the top quark, tau neutrino and Higgs boson, the SM lacks as the complete theory of the fundamental forces for not including gravity. It does not explain matter-antimatter asymmetry (baryon asymmetry), describe accelerating expansion of the universe which could be explained by dark energy. Also the SM does not explain neutrino oscillations and their non-zero masses or explain theory of gravitation.

In the following sections we will describe the SM more deeply. For instance mathematical formulation, underlying symmetries in the SM and particle content.

2.1 Particle content of the Standard Model

All existing matter around us consists of elementary particles, leptons and quarks to be exact [10]. There is total of six quarks and six leptons, electron, muon and tau with each corresponding neutrino. The quarks and leptons can be divided to three generations. The lightest of these are contained in the first generation. Heavier particles decay quicker than the lighter ones. Quarks are paired in three generations as follows: up and down quark, charm and strange quark and for last top and bottom quark. Leptons are paired with corresponding neutrinos in three generations, electron

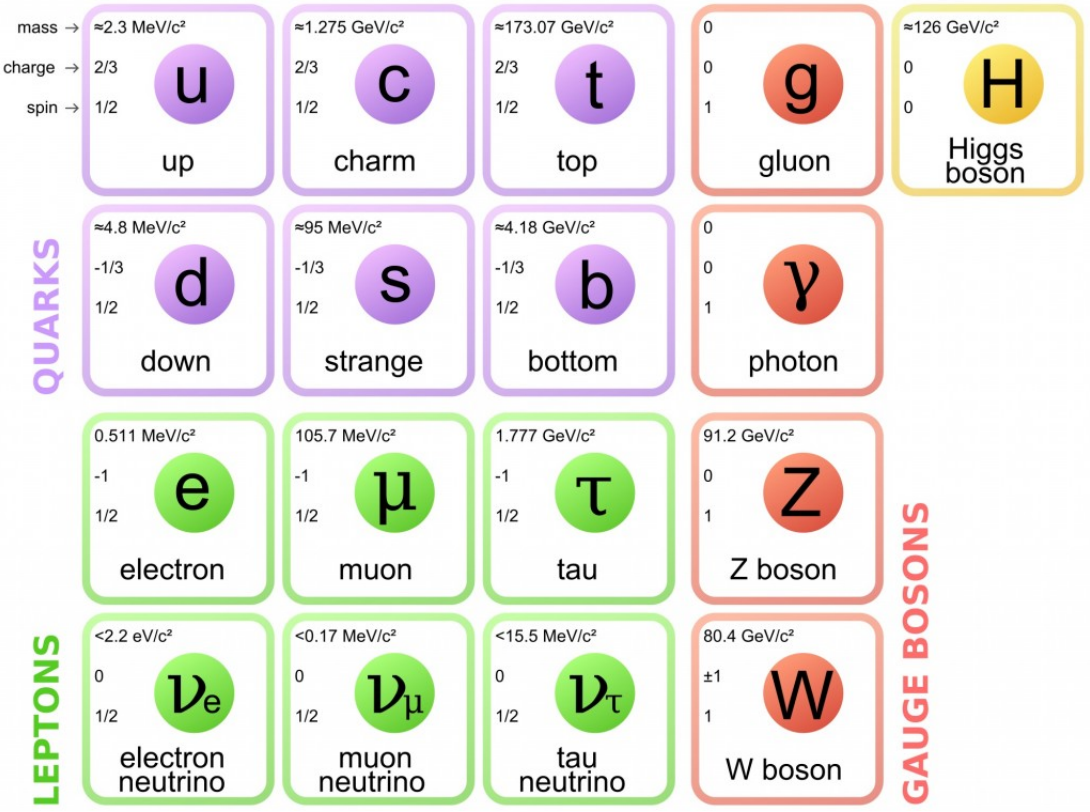

Figure 2.1: Elementary particles of the Standard Model [11].

and electron neutrino, muon and muon neutrino and tau and tau neutrino. Electron, muon and tau have a negative charge but neutrinos are almost massless and neutral in charge.

The interactions between particles are mediated by gauge bosons which are force-carrier particles. Each interaction has its own corresponding gauge boson. Electromagnetic force is carried by photon, strong interaction by gluons, weak interaction by W^+, W^- or Z bosons. The force-carrier of the gravity, "graviton" is yet to be found. Quarks, leptons and gauge bosons are illustrated in the Figure 2.1. The particles interact with each other with gauge bosons. Neutrinos interact only via weak interaction i.e. W or Z boson. Quarks can interact with photon, gluon or W and Z bosons. Leptons like electrons can not interact via strong interaction so they interact with photon or weak gauge bosons. Furthermore the bosons can interact with each other like Higgs or Z bosons and gluons. These interactions are represented in the Figure 2.2.

2.2 Quantum electrodynamics

Quantum electrodynamics (QED) is a relativistic quantum field theory of electrodynamics in particle physics. It describes how matter and light interact with each other.

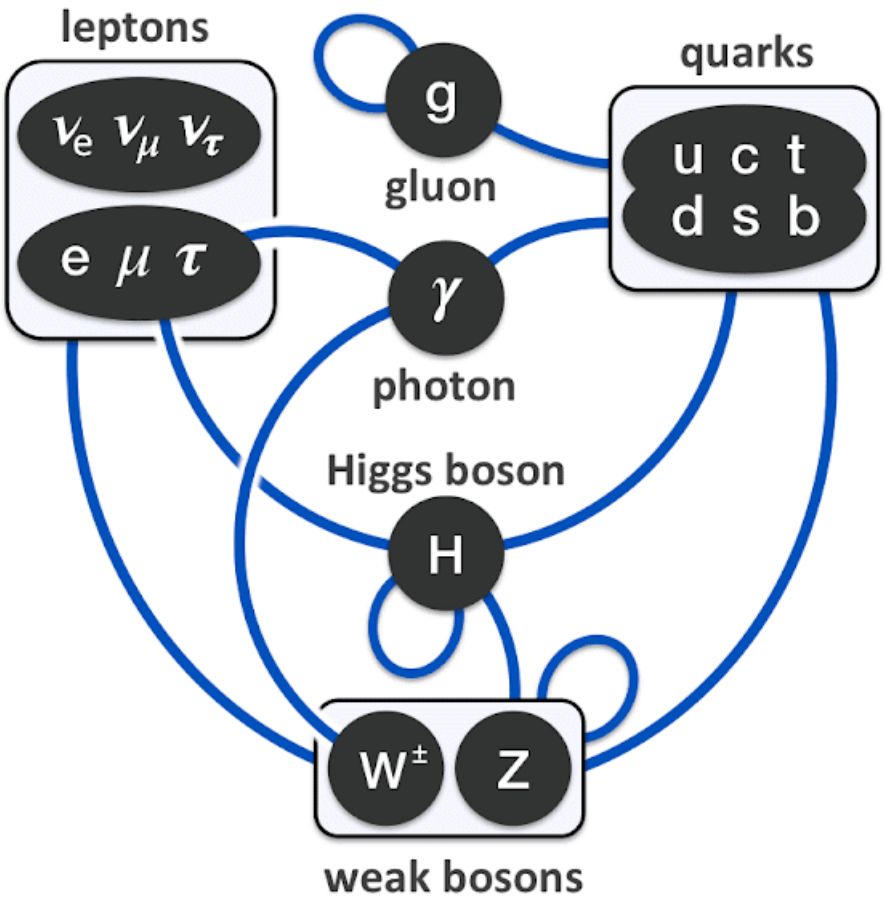

Figure 2.2: Summary of interactions between particles in the Standard Model [15].

It satisfies both principles of quantum mechanics and special relativity. QED is a mathematical description of electrically charged particles interaction via virtual photons.

The QED was developed by several physicists like Dirac, Feynman, Schwinger and Tomonaga but major contribution came from Dirac by his description of radiation and matter interaction and using an ensemble of harmonic oscillators to describe the quantization of the electromagnetic field by introducing creation and annihilation operators of particles [12], [13].

Schwinger took account the self energy of the electron which can be added to regular mass of the electron. The Hamiltonian transforms slightly due to this effect and small correction arises to the electron mass. Then electron mass and charge can be renormalized from the interaction of radiation and matter. This correction is used for the electron in the external magnetic field and it is measured with high precision. This is applied to hydrogen and deuterium atoms hyperfine structure with accurate results. Still there is a slight disagreement with the theory and experimental data [14].

2.2.1 Gauge invariance of the QED

Dirac gave the quantum mechanical description for the spin-$\frac{1}{2}$ charged particles. He combined special relativity and quantum mechanics to produce the Dirac equation

$$(i\gamma^\mu\partial_\mu - m)\psi = 0, \tag{2.1}$$

where γ^μ are the Dirac matrices and m is the mass of the electron. The Dirac equation comes with the four-component spinor $\psi(x)$ which includes both particles and antiparticles. The Dirac equation arises from the Euler-Lagrange equation. By introducing the Dirac Lagrangian for the spinor field $\psi(x)$ by satisfying free-particle Dirac equation

$$\mathcal{L}_D = i\overline{\psi}\gamma^\mu\partial_\mu\psi - m\overline{\psi}\psi = \overline{\psi}(i\not{\partial} - m)\psi, \tag{2.2}$$

from which Feynman notation is used $\not{\partial} = \gamma^\mu\partial_\mu$. Now using Euler-Lagrange equation of fields for the $\overline{\psi}$

$$\partial_\mu\left(\frac{\partial\mathcal{L}_D}{\partial(\partial_\mu\overline{\psi})}\right) - \frac{\partial\mathcal{L}_D}{\partial\overline{\psi}} = 0 \tag{2.3}$$

and consequently the spinor field ψ satisfies the Dirac equation

$$(i\gamma^\mu\partial_\mu - m)\psi = 0. \tag{2.4}$$

The QED is a gauge theory with the symmetry group of $U(1)$. By performing a gauge transformation for the adjoint spinor $\overline{\psi}$ and spinor ψ as follows

$$\psi \to \psi' \quad = e^{-ig_e\alpha}\psi, \tag{2.5}$$
$$\overline{\psi} \to \overline{\psi}' \quad = e^{ig_e\alpha}\psi, \tag{2.6}$$

where g_e and α are constants. Using transformations (2.5) and (2.6) and applying them in the Dirac Lagrangian, the equation (2.2) gives

$$\begin{aligned}\mathcal{L}_D \to \mathcal{L}'_D &= \overline{\psi}'(i\not{\partial} - m)\psi' \\ &= e^{ig_e\alpha}\overline{\psi}(i\not{\partial} - m)\psi e^{-ig_e\alpha} \\ &= e^{-ig_e\alpha}e^{ig_e\alpha}\overline{\psi}(i\not{\partial} - m)\psi \\ &= \overline{\psi}(i\not{\partial} - m)\psi \\ &= \mathcal{L}_D\end{aligned}$$

and therefore Dirac Lagrangian is invariant under global $U(1)$ transformations. Now consider a *local* transformation for the spinor $\psi(x)$

$$\psi(x)' = e^{-ig_e\alpha(x)}\psi(x), \tag{2.7}$$

where g_e is now a strength parameter (electromagnetic coupling constant). By looking the second term $(m\overline{\psi}\psi)$ of the Dirac Lagrangian $\mathcal{L}_D$ in equation (2.2), it is clearly invariant under local gauge transformation. The first term is not since by the definition ψ is formed to transform differently than x and $\partial_\mu\psi$ depends on the neigbourhood of x. Applying the local transformation represented in the equation (2.7) to $\partial_\mu\psi(x)$

$$\partial_\mu\psi' = \partial_\mu e^{-ig_e\alpha}\psi = e^{-ig_e\alpha}[\partial_\mu - ig_e(\partial_\mu\alpha)]\psi \neq e^{-ig_e\alpha}\partial_\mu\psi. \tag{2.8}$$

Thus $\mathcal{L}_D$ is not locally gauge invariant in $U(1)$. In order to restore the gauge invariance, a covariant derivative must to be defined which is gauge invariant in local transformations. The covariant derivative satisfies the condition

$$D_\mu\psi \to D'_\mu\psi' = e^{-ig_e\alpha}D_\mu\psi. \tag{2.9}$$

This form is obtained by introducing a gauge field A^μ as follows

$$D_\mu\psi = (\partial_\mu + ig_eA_\mu)\psi. \tag{2.10}$$

The A_μ transforms as

$$A'_\mu = A_\mu + \partial_\mu \alpha. \tag{2.11}$$

Now calculating $D'_\mu \psi'$ yields

$$D'_\mu \psi' = (\partial_\mu + ig_e A'_\mu) e^{-ig_e \alpha} \psi = e^{-ig_e \alpha} (\partial_\mu + ig_e A_\mu) \psi = e^{-ig_e \alpha} D_\mu \psi. \tag{2.12}$$

Thus the Lagrangian $\mathcal{L}_D$ is locally gauge invariant. Applying the gauge transformation to the Dirac Lagrangian $\mathcal{L}_D$ (2.2)

$$\begin{aligned}
\mathcal{L}_D \to \mathcal{L}'_D &= i\overline{\psi}\gamma^\mu D_\mu \psi - m\overline{\psi}\psi \\
&= i\overline{\psi}\gamma^\mu \partial_\mu \psi - m\overline{\psi}\psi - g_e(\overline{\psi}\gamma^\mu \psi) A_\mu \\
&= \overline{\psi}(i\partial\!\!\!/ - m)\psi - g_e(\overline{\psi}\gamma^\mu \psi) A_\mu \\
&= \mathcal{L}_D - g_e(\overline{\psi}\gamma^\mu \psi) A_\mu \qquad (2.13) \\
&= \mathcal{L}_D + \mathcal{L}_{int}. \qquad (2.14)
\end{aligned}$$

New term appeared due to covariant derivative in (2.13), which we shall call the interaction term denoted by $\mathcal{L}_{int}$. So far we have found the way to describe charged leptons coupled with the photons with the interaction term $\mathcal{L}_{int}$. The interaction term electrons and positrons are created or destroyed with each other but photons can be created or destroyed singly. These two events can be illustrated with Feynman diagrams in the Figure 2.3.

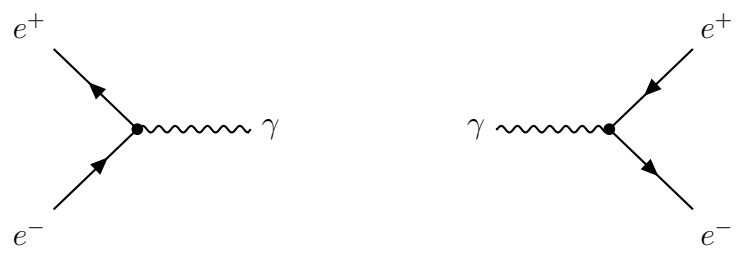

Figure 2.3: Pair production in QED: on the left electron-positron annihilation and on the right creation of positron and electron from the photon.

Now the fermion coupling is described by Dirac Lagrangian $\mathcal{L}_D$ and interactions between fermions and photons is described by the interaction term $\mathcal{L}_{int}$. The QED Lagrangian does not yet describe electromagnetic field interaction. The kinetic term for the gauge field A_μ is needed which is quadratic in the derivative of the field and preserving gauge invariance of the Lagrangian. By introducing the electromagnetic field tensor

$$F_{\mu\nu} = \partial_\mu A_\nu - \partial_\nu A_\mu, \tag{2.15}$$

where A_μ is a photon field. This is clearly invariant quantity thus can be added to Lagrangian by contracting Lorentz indices. This term can be represented as $CF_{\mu\nu}F^{\mu\nu}$ where the constant C is chosen to be $\frac{1}{4}$ for the convenience. The desired term is now quadratic in the derivative and Euler-Lagrange equations match the relativistic formulation of the Maxwell equations. Now we have full description of the interactions in QED. Thus the QED Lagrangian $\mathcal{L}_{QED}$ has the form

$$\begin{aligned}\mathcal{L}_{QED} &= -\frac{1}{4}F_{\mu\nu}F^{\mu\nu} + \overline{\psi}(i\partial\!\!\!/ - m)\psi - g_e(\overline{\psi}\gamma^\mu\psi)A_\mu \\ &= \mathcal{L}_{EM} + \mathcal{L}_D + \mathcal{L}_{int}.\end{aligned}$$

2.3 Quantum chromodynamics

Quantum chromodynamics (QCD) is a theory that describes strong interaction between gluons and quarks. The QCD is constructed with same analogy as the QED. Instead of photon, the QCD force-carrier particle is called a gluon which transmits the strong force between particles of matter that carry a colour charge. Therefore the strong interaction is limited only to subatomic particles, quarks that form hadrons such as protons, neutron and mesons (composed of a quark and an antiquark). Gluons can self-interact with each other but in QED photons can not.

2.3.1 Gauge invariance of the QCD

The QED had the $U(1)$ local gauge invariance. Now in QCD this is not the case, the corresponding gauge invariance is obtained in $SU(3)$ local phase transformations [16],

$$\psi(x) \to \psi'(x) = e^{ig_s\alpha(x)\cdot\hat{T}}\psi(x), \tag{2.16}$$

where $\alpha^a(x)$ are eight functions of the space-time coordinate x that are related to the generators of the symmetry group $SU(3)$ which are $\hat{T} = \{T^a\}$. These generators can be expressed as eight Gell-Mann matrices

$$T^a = \frac{1}{2}\lambda^a, \tag{2.17}$$

which can be explicitly written as

$$\lambda_1 = \begin{pmatrix} 0 & 1 & 0 \\ 1 & 0 & 0 \\ 0 & 0 & 0 \end{pmatrix}, \quad \lambda_2 = \begin{pmatrix} 0 & -i & 0 \\ i & 0 & 0 \\ 0 & 0 & 0 \end{pmatrix}, \quad \lambda_3 = \begin{pmatrix} 1 & 0 & 0 \\ 0 & -1 & 0 \\ 0 & 0 & 0 \end{pmatrix},$$

$$\lambda_4 = \begin{pmatrix} 0 & 0 & 1 \\ 0 & 0 & 0 \\ 1 & 0 & 0 \end{pmatrix}, \quad \lambda_5 = \begin{pmatrix} 0 & 0 & -i \\ 0 & 0 & 0 \\ i & 0 & 0 \end{pmatrix}, \quad \lambda_6 = \begin{pmatrix} 0 & 0 & 0 \\ 0 & 0 & 1 \\ 0 & 1 & 0 \end{pmatrix},$$

$$\lambda_7 = \begin{pmatrix} 0 & 0 & 0 \\ 0 & 0 & -i \\ 0 & i & 0 \end{pmatrix} \quad \text{and} \quad \frac{1}{\sqrt{3}} \begin{pmatrix} 1 & 0 & 0 \\ 0 & 1 & 0 \\ 0 & 0 & -2 \end{pmatrix}.$$

The additional degrees of freedom of the wave function ψ is caused by 3×3 matrix representation of $SU(3)$ generators. The additional degree of freedom is called colour with three different states labelled by red, green or blue. The local gauge transformation of the $SU(3)$ can be interpreted as rotation of the states in the colour space. By applying the transformation to the Dirac equation, it becomes

$$i\gamma^\mu \left[\partial_\mu + ig_s(\partial_\mu\alpha)\cdot\hat{T}\right]\psi = m\psi. \tag{2.18}$$

To keep the Dirac equation gauge invariant in the local transformations, eight new fields needs to be introduced as G^a_μ, where each G^a_μ corresponds the generators of the group $SU(3)$. Defining the covariant derivative D_μ as

$$D_\mu = \partial_\mu + ig_s T^a G^a_\mu, \tag{2.19}$$

allows us write the Dirac equation as follows

$$i\gamma^\mu D_\mu \psi - m\psi = 0. \tag{2.20}$$

In order to Lagrangian be invariant under local transformations, the gauge transformation needs to be introduced

$$G^k_\mu \to G^{k'}_\mu = G^k_\mu - \partial_\mu \alpha_k - g_s f_{ijk} \alpha_i G^j_\mu. \tag{2.21}$$

The term $g_s f_{ijk} \alpha_i G^j_\mu$ appeared since the generators of the $SU(3)$ does not commute and the structure constants f_{ijk} are defined with the commutation relations $[\lambda_i, \lambda_j] = 2i f_{ijk} \lambda_k$. Because of this relation, the QCD is a non-Abelian gauge theory. The additional term gives rise to the gluon self-interaction which is illustrated in the Figure 2.4. The gluons are the eight new fields G^a, thus we can form the qqg interaction vertex

$$g_s T^a \gamma^\mu G^a_\mu \psi = g_s \frac{1}{2} \lambda^a \gamma^\mu G^a_\mu \psi. \tag{2.22}$$

Using commutator of two covariant derivatives to compute gluon field tensor $G^k_{\mu\nu}$,

$$G^k_{\mu\nu} = \partial_\mu G^k_\nu - \partial_\nu G^k_\mu + g_s f_{ijk} G^j_\mu G^k_\nu. \tag{2.23}$$

The complete QCD Lagrangian is then given by

$$\mathcal{L}_{QCD} = \overline{\psi} \left(i \not{D} - m \right) \psi - \frac{1}{4} G^k_{\mu\nu} G^{\mu\nu k}, \tag{2.24}$$

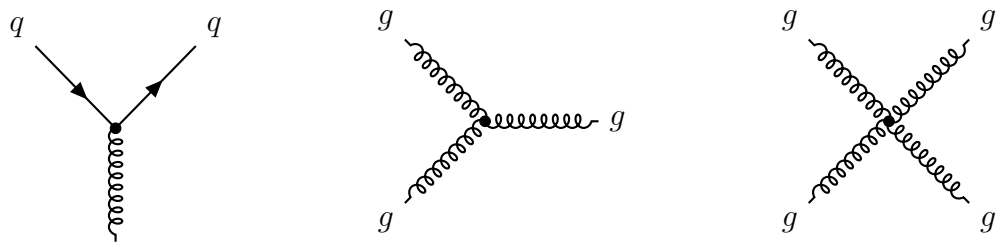

Figure 2.4: Quark-gluon scattering and gluon self-interaction.

where $\frac{1}{4}G^k_{\mu\nu}G^{\mu\nu k}$ is the kinetic term of the gluon field and $\psi(x)$ is the quark field.

2.3.2 Gluons and colour

The structure of the QED is similar to QCD. In QED the interaction is mediated by single generator of $U(1)$ in local gauge symmetry which corresponds a massless photon. In QCD there is eight gluons which correspond the generators of the $SU(3)$. The single charge in QED is replaced by three red, green and blue colour charges which are orthogonal states. Only the particles that carry a non-zero colour charge can couple with gluons. This means that leptons i.e. electrons can not couple with the gluons and have strong interaction. Like in QED the antiparticles have an opposite electric charge compared to particles. By similar manner the antiquarks have an opposite colour charge to quarks, $\overline{r}$, $\overline{g}$, $\overline{b}$. The colour states can be expressed in the orthogonal basis as three dimensional wave functions

$$r = \begin{pmatrix} 1 \\ 0 \\ 0 \end{pmatrix}, \quad g = \begin{pmatrix} 0 \\ 1 \\ 0 \end{pmatrix} \text{ and } \quad b = \begin{pmatrix} 0 \\ 0 \\ 1 \end{pmatrix} \tag{2.25}$$

The gauge invariance in local transformations of $SU(3)$ implies conservation of the colour charge. By comparing QCD qqg vertex interaction given in equation (2.22) and QED interaction term

$$-ig_e\gamma^\mu A_\mu\psi \rightarrow -ig_s\frac{1}{2}\lambda^a\gamma^\mu G^a_\mu\psi.$$

Now the vertex factor of the QCD can be identified as

$$-ig_s\gamma^\mu \rightarrow -ig_s\gamma^\mu \frac{1}{2}\lambda^a.$$

The interaction differs only by the Gell-Mann matrices in the QCD interaction, which can only act quark wave function that have a colour charge. The Feynman diagrams of the strong interaction can be constructed by labelling quarks with colour and gauge invariant gluon fields G^ν_μ that corresponds the generators of the $SU(3)$ [17]. There is no restriction for quarks interacting with same or different colour. The coupling in the QCD vertex is given by the coefficient that corresponds gluon four-potential for the process that appears in the gluon matrix which is given by

$$\sum_{k=1}^{8} g_s G^\mu_k \frac{\lambda_k}{2} = \frac{1}{\sqrt{2}} \begin{pmatrix} \frac{1}{\sqrt{2}}G^\mu_3 + \frac{1}{\sqrt{6}}G^\mu_8 & G^\mu_{r\bar{g}} & G^\mu_{r\bar{b}} \\ G^\mu_{g\bar{r}} & -\frac{1}{\sqrt{2}}G^\mu_3 + \frac{1}{\sqrt{6}}G^\mu_8 & G^\mu_{g\bar{b}} \\ G^\mu_{b\bar{r}} & G^\mu_{b\bar{g}} & -\frac{2}{\sqrt{6}}G^\mu_8 \end{pmatrix}. \tag{2.26}$$

For instance G^μ_8 has a factor of $\frac{g_s}{2\sqrt{3}}$ and G^μ_3 has a factor of $\frac{g_s}{2}$ in the interaction of two red quarks. When different colour quarks interact, the coupling factor can change. For the interaction $rb \rightarrow rb$ the coupling factor for the red quark is $\frac{g_s}{2\sqrt{3}}$ and $-\frac{g_s}{\sqrt{3}}$ for the blue. When dealing with the antiquarks the coupling factor flips sign of the corresponding factor. Furthermore, when dealing with electromagnetic interaction, the strength of the interaction is proportional to the product of the two coupling factors $\propto g_s^2$. Defining the colour factor C which is equal to coefficient in front of g_s^2 from the product of the two coupling factors. The sign of the colour factor indicates if the interaction is repulsive or attractive. The negative sign is attractive and positive is repulsive. The colour factor for the process $C(ik \rightarrow jl)$ can be calculated as follows

$$C(ik \rightarrow jl) = \frac{1}{4}\sum_{a=1}^{8} \lambda^a_{ji}\lambda^a_{lk}, \tag{2.27}$$

where λ^a are the Gell-Mann matrices. For the same colour process i.e. $(rr \rightarrow rr)$, the calculation yields

$$C(rr \to rr) = \frac{1}{4}\sum_{a=1}^{8} \lambda_{11}^a \lambda_{11}^a = \frac{1}{4}(\lambda_{11}^3\lambda_{11}^3 + \lambda_{11}^8\lambda_{11}^8) = \frac{1}{4}\left(1 + \frac{1}{3}\right) = \frac{1}{3}. \tag{2.28}$$

Because of the colour symmetry of the group $SU(3)$, it is guaranteed to have same results for all colours r, g and b. Therefore we have the result

$$C(rr \to rr) = C(gg \to gg) = C(bb \to bb) = \frac{1}{3}. \tag{2.29}$$

The colour factor for the process containing different colour quarks i.e. $rb \to rb$ is

$$C(rb \to rb) = \frac{1}{4}\sum_{a=1}^{8} \lambda_{11}^a \lambda_{33}^a = \frac{1}{4}\left(\frac{1}{\sqrt{3}} \cdot \frac{-2}{\sqrt{3}}\right) = -\frac{1}{6}, \tag{2.30}$$

where 11 and 33 are only non-zero terms that contribute to the colour factor. By the $SU(3)$ colour symmetry, other similar processes have the same colour factor,

$$\begin{aligned} &C(rb \to rb) = C(rg \to rg) = C(gr \to gr) \\ &= C(gb \to gb) = C(br \to br) = C(bg \to bg) = -\frac{1}{6} \end{aligned} \tag{2.31}$$

Now for process that reverses the order of the colours $C(ij \to ji)$, the colour factors are,

$$\begin{aligned} &C(rb \to br) = C(rg \to gr) = C(gr \to rg) \\ &= C(gb \to bg) = C(br \to rb) = C(bg \to gb) \\ &= \frac{1}{4}\sum_{a=1}^{8} \lambda_{21}^a \lambda_{12}^a = \frac{1}{4}\left(\lambda_{12}^1\lambda_{21}^1 + \lambda_{12}^2\lambda_{21}^2\right) = \frac{1}{2}, \end{aligned} \tag{2.32}$$

where the only non-zero terms come from the 12 and 21 positions. In the interaction that involves different colours like interaction ($rb \to bg$), it has a colour factor of zero due to fact that none of the λ-matrices has non-zero entries in both ji

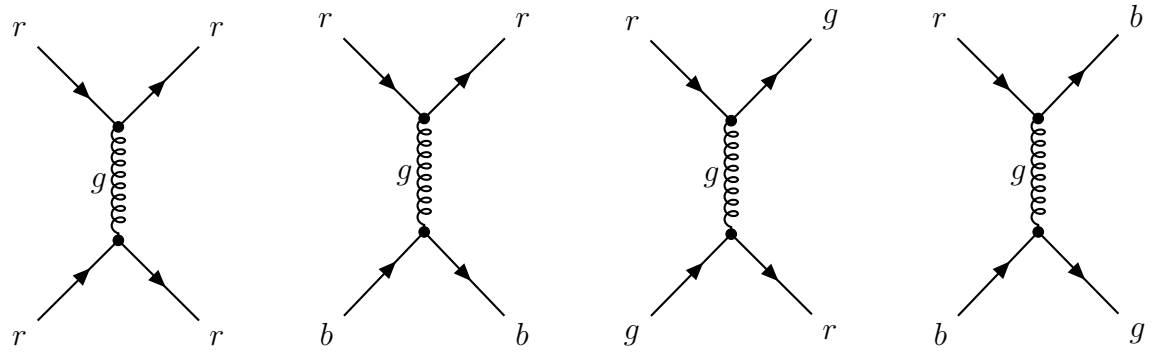

Figure 2.5: Examples of the four different quark-quark scattering.

and lk positions described in the equation (2.27). This leads to colour factor to be zero. These quark-quark interactions are illustrated in the Figure 2.5.

2.4 Electroweak unification and interactions

So far we have discussed gauge theories of the QED and QCD. The QED is the most simple, Abelian quantum field theory (QFT). The difference between QCD and QED is the symmetry groups that correspond the interactions in the both cases. In QED the gauge invariant group is $U(1)$ and in QCD the corresponding group is $SU(3)$ which is a non-Abelian gauge group with eight distinct generators that indicate different gluon fields and quark interactions. The weak interactions differ from both of these theories since it comes in two types, neutral and charged-current interactions, mediated by a Z boson and $W^{\pm}$ bosons. The distinction of these two types of interactions involve different types of couplings between leptons and quarks, the W boson can couple only left-handed fermions and change flavour in the interactions unlike the Z boson that can couple with either left-handed or right-handed fermions. Furthermore the electroweak theory is a chiral, non-Abelian gauge theory which symmetry can be spontaneously broken [18].

The term *chirality* refers to left- and right-handedness of a particle. The chiral states of the fermions can be constructed by introducing projection operators

$$P_R = \frac{1}{2}\left(1+\gamma^5\right), \quad P_L = \frac{1}{2}\left(1-\gamma^5\right), \tag{2.33}$$

where $\gamma^5 \equiv i\gamma^0\gamma^1\gamma^2\gamma^3$. In a chiral gauge theory, the left-handed and right-handed fermions are defined by

$$\psi_L = P_L\psi_L = \frac{1}{2}\left(1-\gamma^5\right)\psi_L, \quad \psi_R = P_R\psi_R = \frac{1}{2}\left(1+\gamma^5\right)\psi_R. \tag{2.34}$$

There is total of seven different chiral spinors for a one generation of the particles: one left-handed for neutrino and both left- and right-handed for quarks and the charged lepton i.e. electron. Electroweak gauge group is constructed by taking a direct product of the groups $U(1)$ and $SU(2)$, so that $G_{EW} = SU(2)_W \times U(1)_Y$, where subscript Y stands for a hypercharge and W for weak isospin. The corresponding assignment of the quantum numbers grouping into representations of the gauge group is obtained in the following way: The group $SU(2)$ has a one dimensional singlet representation and also higher dimensional representations starting with the two dimensional doublet. Leptons and quarks are not allowed to mix due to fact that the colour does not change nor the handedness of the fields under weak interactions. If that were to happen it would violate Lorentz symmetry. The Abelian factor, $U(1)_Y$ has only one-dimensional representations and therefore it is possible to assign different hypercharges to the singlets and doublets of $SU(2)_W$.

Neutrinos interact only with left-handed fermions. The interactions are mediated by $W^\pm$ and Z bosons and the $W^\pm$ bosons couple only with left-handed fermions ψ_L. These conditions indicate that right-handed fields has to be form of a singlet and left-handed fields doublet states from u_L and d_L for quarks and for leptons from e_L and ν_L. Thus the multiplets for the $SU(2)_W$ can be constructed as follows

$$q_L = \begin{pmatrix} u_L \\ d_L \end{pmatrix}, \qquad l_L = \begin{pmatrix} \nu_L \\ e_L \end{pmatrix}, \qquad u_R, \qquad d_R, \qquad e_R, \tag{2.35}$$

with the corresponding hypercharges of the fields

$$\text{field: } q_L \quad u_R \quad d_R \quad l_L \quad e_R \tag{2.36}$$

$$\text{hypercharge: } \frac{1}{6} \quad \frac{2}{3} \quad -\frac{1}{3} \quad -\frac{1}{2} \quad -1, \tag{2.37}$$

where the hypercharges are determined from electric charge and isospin of the quarks $Y = Q - I^3$. Only the left-handed fermions have non-zero isospin I^3. The hypercharge

for singlets u_R, d_R, e_R is same as their electric charge. The isospin $I^3 = \pm\frac{1}{2}$ of the left-handed fermion is assigned with same sign as their electric charge, from which we obtain the hypercharges in (2.37). The gauge group $SU(2)_W$ has three distinct generators, which can be chosen to be the Pauli spin matrices σ^i. They are defined as

$$\sigma^1 = \begin{pmatrix} 0 & 1 \\ 1 & 0 \end{pmatrix}, \qquad \sigma^2 = \begin{pmatrix} 0 & -i \\ i & 0 \end{pmatrix}, \qquad \sigma^3 = \begin{pmatrix} 1 & 0 \\ 0 & -1 \end{pmatrix} \tag{2.38}$$

and three gauge fields W_μ^I, $I = 1, 2, 3$. A gauge field that corresponds the group $U(1)_Y$ is B_μ. Now the covariant derivative can be defined for the left-handed fields as

$$D_\mu \psi_L = \left(\partial_\mu + ig\widetilde{W}_\mu + ig'YB_\mu\right)\psi_L, \tag{2.39}$$

where $\widetilde{W}_\mu = \frac{1}{2}\sigma^I W_\mu^I$. The right-handed fields do not couple with the W bosons due to a fact that right-handed fields are singlets under the group $SU(2)_W$. The corresponding covariant derivative for the right-handed fields is then

$$D_\mu \psi_R = \left(\partial_\mu + ig'YB_\mu\right)\psi_R. \tag{2.40}$$

We need to transform the fields $D_\mu\psi$ same way as the fields ψ in the $SU(2)_L \times U(1)_Y$ gauge transformation, the gauge transformation is needed for thee fields B_μ and W_μ [19]

$$B_\mu \to B'_\mu = B_\mu + \frac{1}{g'}\partial_\mu \alpha(x), \tag{2.41}$$

$$\widetilde{W}_\mu \to \widetilde{W}'_\mu = U_L(x)\widetilde{W}_\mu U_L^\dagger(x) - \frac{i}{g}\partial_\mu U_L(x) U_L^\dagger(x), \tag{2.42}$$

where $U_L(x) = e^{i\frac{\sigma_j}{2}\alpha^j(x)}$, $j = 1, 2, 3$, is the generator of the group $SU(2)_L$. We see that the gauge transformation for the field B_μ corresponds gauge transformation for the photon in QED and the coupling of the field ψ to B_μ is also free like in QED. Fields W_μ^i are gauge invariant under $SU(2)_L$ transformations like the gluon fields in QCD. This implies that the Dirac Lagrangian is invariant under local gauge transformations. The gauge-invariant kinetic terms for the fields B_μ and W_μ are obtained by using commutation relations for the fields and representing the B_μ in the form of the

electromagnetic field tensor $F_{\mu\nu}$,

$$B_{\mu\nu} = \partial_\mu B_\nu - \partial_\nu B_\mu, \tag{2.43}$$

$$\widetilde{W}_{\mu\nu} = \frac{i}{g}\left[\left(\partial_\mu - ig\widetilde{W}_\mu\right), \left(\partial_\nu - ig\widetilde{W}_\nu\right)\right] = \partial_\mu \widetilde{W}_\nu - \partial_\nu \widetilde{W}_\mu - ig\left[W_\mu, W_\nu\right], \tag{2.44}$$

$$\widetilde{W}_{\mu\nu} = \frac{\sigma_i}{2} W^i_{\mu\nu}, \qquad W^i_{\mu\nu} = \partial_\mu W_\nu - \partial^i_\nu W^i_\mu + g\epsilon^{ijk} W^j_\mu W^k_\nu. \tag{2.45}$$

With these relations we obtain normalized kinetic Lagrangian

$$\mathcal{L}_{kin} = -\frac{1}{4} B_{\mu\nu} B^{\mu\nu} - \frac{1}{2} Tr\left[\widetilde{W}_{\mu\nu}\widetilde{W}^{\mu\nu}\right] = -\frac{1}{4} B_{\mu\nu} B^{\mu\nu} - \frac{1}{4} W^i_{\mu\nu} W^{\mu\nu}_i. \tag{2.46}$$

The Lagrangian gives rise to gauge field self-interactions of cubic and quartic order due to quartic terms in the gauge field $W^i_{\mu\nu}$. These self- interactions are illustrated in the Figure 2.6.

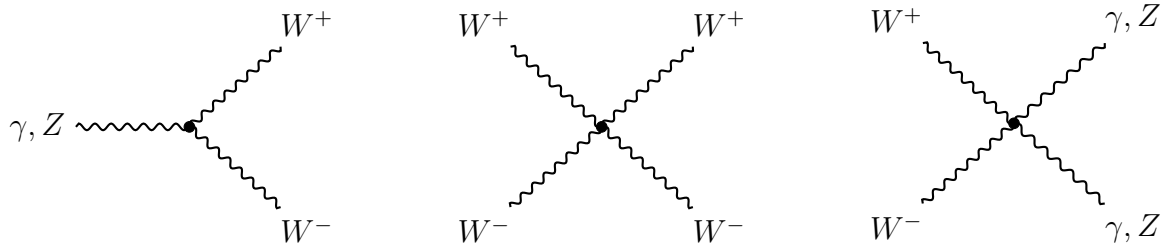

Figure 2.6: Self-interaction vertices of the gauge boson.

Gauge bosons do not have the mass term since the gauge symmetry prevents it. Fermion mass term cannot either be written due to couplings with both right- and left-handed fields since electroweak interactions are only possible for the left-handed fermions. This means that fermion mass term violates $SU(2)$ gauge symmetry. Weak interactions mediated by W^+ and W^- bosons change flavour. In the case of quarks, the up type quark is transformed into a down type quark and vice versa. Illustration of the charged-current weak interaction is provided in the Figure 2.7.

Fermions can also interact via neutral-current interactions which involve neutral gauge fields W^3_μ and B_μ. These fields can be identified as a photon γ and Z boson.

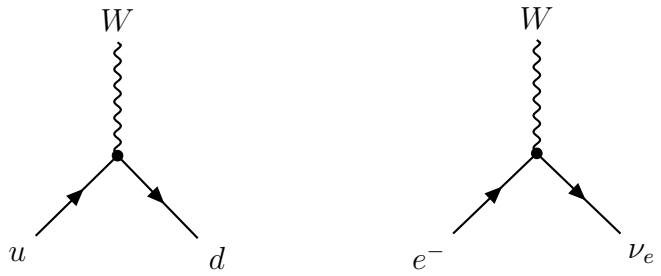

Figure 2.7: Charged-current weak interaction of quarks and leptons.

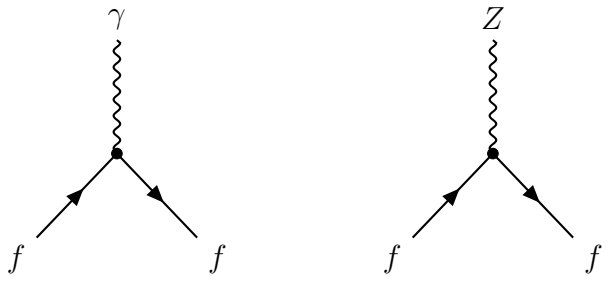

Figure 2.8: Neutral-current interaction mediated by a photon and the Z boson.

The neutral-current interaction does not change flavour. Photon interacts same way to both chirality states of the fermions and therefore the gauge boson B_μ cannot be interpreted as the electromagnetic field. Neutral-current interactions are described by Feynman diagrams in the Figure 2.8.

Furthermore the mixing of the fields W_μ^3 and B_μ can be expressed as in terms of fields A_μ and Z_μ and the weak mixing angle θ_W

$$\begin{pmatrix} W_\mu^3 \\ B_\mu \end{pmatrix} = \begin{pmatrix} \cos\theta_W & \sin\theta_W \\ -\sin\theta_W & \cos\theta_W \end{pmatrix} \begin{pmatrix} Z_\mu \\ A_\mu \end{pmatrix}. \tag{2.47}$$

The gauge bosons A_μ and Z_μ are linear combinations of the fields W_μ^3 and B_μ and couplings g and g',

$$W_\mu^\pm = \frac{W_\mu^1 \mp iW_\mu^2}{\sqrt{2}}, \quad Z_\mu = \frac{gW_3 - g'B_\mu}{\sqrt{g^2+g'^2}} = W_\mu^3 \cos\theta_W - B_\mu \sin\theta_W, \tag{2.48}$$

$$A_\mu = \frac{g'W_\mu^3 + gB_\mu}{\sqrt{g^2+g'^2}} = W_\mu^3 \sin\theta_W + B_\mu \cos\theta_W, \tag{2.49}$$

from which the A_μ can be interpreted as the electromagnetic field. [20]

Chapter 3

Higgs mechanism

The Higgs mechanism is one the most important theories in the Standard Model. It explains how the particles and gauge bosons i.e. W or Z bosons acquire their mass without breaking gauge theory. The mechanism was developed by Peter Higgs, Robert Brout and François Englert in the 1960s and they won the Nobel price in 2013 by the discovery of the Higgs boson based on Higgs publication related to gauge boson masses [6].

3.1 Real scalar field

To understand this mechanism we first consider a simple toy model which is one dimensional respect to scalar field ϕ. After that we define the potential $V(\phi)$ using ϕ^4 theory and Lagrangian $\mathcal{L}$ using the formalism of the QFT. In ϕ^4 theory the potential has the form [21]

$$V(\phi) = \frac{1}{2}\mu^2\phi^2 + \frac{\lambda}{4}\phi^4, \tag{3.1}$$

where $\lambda > 0$ and μ is an arbitrary constant. Now we can write down the Lagrangian by using the formalism of the QFT including the kinetic term of the scalar field $\frac{1}{2}(\partial_\mu\phi)(\partial^\mu\phi)$. The Lagrangian is then

$$\mathcal{L} = \frac{1}{2}\left(\partial_\mu \phi\right)\left(\partial^\mu \phi\right) - V(\phi)$$

$$= \frac{1}{2}\left(\partial_\mu \phi\right)\left(\partial^\mu \phi\right) - \frac{1}{2}\mu^2\phi^2 - \frac{\lambda}{4}\phi^4. \tag{3.2}$$

By looking at the potential term, we notice that the form of the potential depends on the values of μ^2. If $\mu^2 > 0$, the potential has only one minimum value at point $\phi = 0$, but if $\mu^2 < 0$, it has two minima at points

$$\phi = \pm v = \pm \left| \frac{\sqrt{-\mu^2}}{\lambda} \right|. \tag{3.3}$$

The potentials of different cases are shown in the Figure 3.1.

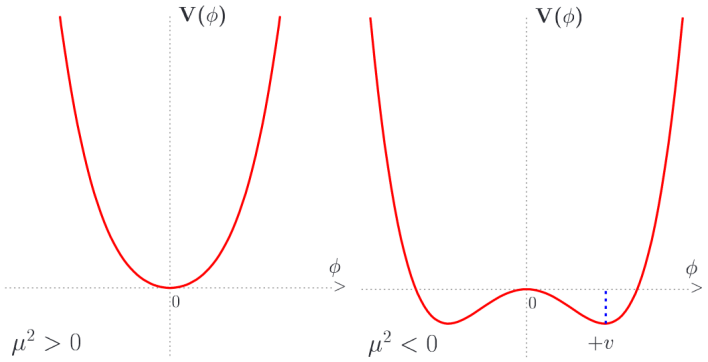

Figure 3.1: Potential V(ϕ) of the scalar field ϕ where $\mu^2 > 0$ (left) and $\mu^2 < 0$ (right) [21].

The values for field ϕ in the equation (3.3) are the vacuum expectation values (vev). To find the energies of the particles in this potential, we choose the case $\phi = v$ and investigate the behaviour around the minimum of the potential $V(\phi)$. We need to introduce a new scalar field h such that $\phi = v + \eta$ and the vacuum state of this new field h is zero i.e. $\langle 0|\eta|0\rangle = 0$. Now we expand the scalar field h in the form of Lagrangian around the minimum $\eta = 0$. This yields an extra interaction and self-interaction terms for the field h. Writing them in the form of the Lagrangian in equation (3.2) gives

$$\mathcal{L} = \frac{1}{2}(\partial_\mu\eta)(\partial^\mu\eta) - \frac{\mu^2}{2}\left(v^2 + 2v\eta + \eta^2\right) - \frac{\lambda}{4}\left(v^4 + 4v^3\eta + 6v^2\eta^2 + 4v\eta^3 + \eta^4\right)$$

$$= \frac{1}{2}(\partial_\mu\eta)(\partial^\mu\eta) - \frac{v^2}{2}\left(\mu^2 + \frac{\lambda v^2}{2}\right) - v\eta\left(\mu^2 + \lambda\eta^2\right) - \frac{\eta^2}{2}\left(\mu^2 + 3v^2\lambda\right) - \lambda v\eta^3 - \frac{\lambda}{4}\eta^4. \tag{3.4}$$

By using the relation $\mu^2 = -\lambda v^2$, we see that linear term cancels out and we are left with

$$\mathcal{L} = \frac{1}{2}(\partial_\mu\eta)(\partial^\mu\eta) - \lambda v^2\eta^2 - \lambda v\eta^3 - \frac{\lambda}{4}\eta^4 + \frac{\lambda v^4}{4}. \tag{3.5}$$

We identify the mass term of the scalar field η as $m_\eta^2 = 2\lambda v^2 = -2\mu^2$. The terms η^3 and η^4 are cubic and quartic self-interaction terms and are illustrated in the Figure 3.2.

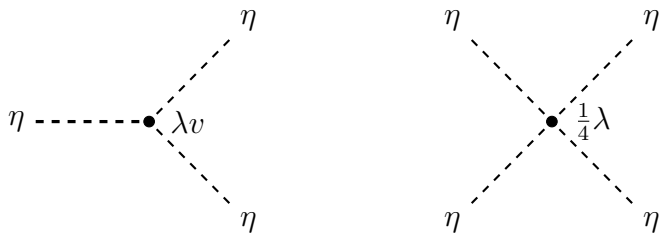

Figure 3.2: Cubic and quartic self-interactions of the scalar field η.

The mass term m_η was generated from self-interactions of the field η. By simply comparing the Lagrangians from the equations (3.2) and (3.5), we see that the initial Lagrangian has only even power terms respect to the scalar field ϕ and the Lagrangian in the equation (3.5) has one cubic term in terms of η. This means that the initial Lagrangian is symmetric under transformation $\phi \to -\phi$. This is simply called parity transformation. But applying parity transformation to the field η does not work. The symmetry is broken and we cannot apply $\eta \to -\eta$ anymore. This is a simple example of the *spontaneous symmetry breaking* (SSB) which we will use in next section with the complex scalar fields. After the SSB occurs, one has to choose one of the other vacuum states, $\phi_1 = v$ or $\phi_2 = -v$. After this decision we have only one unique vacuum state without symmetric properties of the initial Lagrangian. The potential of the Lagrangian with the field η is then

$$V(\eta) = \lambda v^2\eta^2 + \lambda v\eta^3 + \frac{\lambda}{4}\eta^4 - \frac{\lambda}{4}v^4. \tag{3.6}$$

We notice that the potential has theoretically a minimum at $\eta \neq 0$, but this ruins the condition where $\langle 0|\eta|0\rangle = 0$. By applying extremum condition to the potential $V(\eta)$, we obtain

$$\frac{\partial V}{\partial \eta} = \lambda\eta\left(\eta^2 + 3v\eta + 2v^2\right) = \lambda\eta\left(\eta + v\right)\left(\eta + 2v\right) = 0. \tag{3.7}$$

The potential $V(\eta)$ has 3 extrema at points $\eta = 0, \eta = -v$ and $\eta = -2v$. Corresponding values are then

$$\begin{cases} V(\eta = 0) = -\frac{\lambda v^4}{4} < 0 \\ V(\eta = -v) = \lambda v^4(1 - 1 + 1/4 - 1/4) = 0 \\ V(\eta = -2v) = \lambda v^4(4 - 8 + 16/4 - 1/4) = V(\eta = 0) = -\frac{\lambda v^4}{4} < 0. \end{cases} \tag{3.8}$$

We have one extremum at $\eta = -v$ and two minima that share same value $-\frac{\lambda v^4}{4}$ at points $\eta = 0$ and $\eta = -2v$. Since there is two minima with same depths we can choose one of them to be the true vacuum state and for the convenience the minima at point $\eta = 0$ is chosen since it satisfies our desired condition $\langle 0|\eta|0\rangle = 0$.

3.2 Complex scalar field

Now that we have gone through the real scalar field Higgs potential, we can move to the complex scalar field $\phi = \frac{1}{\sqrt{2}}(\phi_1 + i\phi_2)$. As in previous section, the initial Lagrangian has same form but now it is a complex field [21]

$$\mathcal{L} = \frac{1}{2}(\partial_\mu\phi)^*(\partial^\mu\phi) - \mu^2\phi^*\phi - \lambda(\phi^*\phi)^2, \tag{3.9}$$

where $\lambda > 0$. When the transformation $\phi \to \phi' = e^{i\alpha}\phi$ is applied to the Lagrangian, it stays invariant thus it has a global symmetry $U(1)$. Now writing the newly introduced

Higgs potential in terms of ϕ_1 and ϕ_2

$$V(\phi) = \frac{\mu^2}{2}(\phi_1^2 + \phi_2^2) + \frac{\lambda}{4}(\phi_1^2 + \phi_2^2)^2. \tag{3.10}$$

We have two cases for the μ^2, it can be positive or negative. For the case $\mu^2 > 0$, the potential has a minimum when both fields ϕ_1 and ϕ_2 are zero. If $\mu^2 < 0$, we have an infinite set of minima defined as

$$\phi_1^2 + \phi_2^2 = -\frac{\mu^2}{\lambda} = v^2. \tag{3.11}$$

The shape of the potential depends on the sign of μ^2, it becomes paraboloid with non-degenerate minima when both fields are zero for $\mu^2 > 0$. However, when $\mu^2 < 0$, the potential forms "mexican hat" style potential which is illustrated in the Figure 3.3.

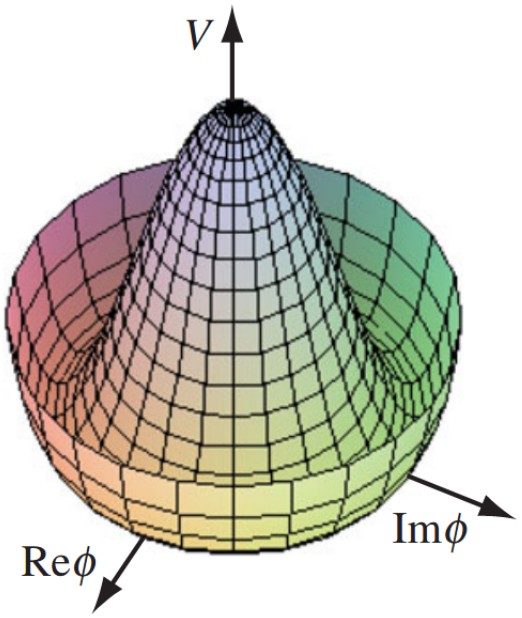

Figure 3.3: Higgs potential for complex scalar field when $\mu^2 < 0$ [22] .

Now in the Mexican hat potential the physical vacuum state corresponds one point on a circle of infinite set of minima breaking the global $U(1)$ symmetry [16]. Since the vacuum state is a circle, we can choose it to be in real direction $(\phi_1, \phi_2) = (v, 0)$. Now by defining fields ϕ_1 and ϕ_2 as $\phi_1(x) = \eta(x) + v$ and $\phi_2(x) = \xi(x)$, the field $\phi(x)$ becomes

$$\phi(x) = \frac{1}{\sqrt{2}}(\eta + v + i\xi). \tag{3.12}$$

The Lagrangian immediately takes form

$$\mathcal{L} = \frac{1}{2}(\partial_\mu \eta)(\partial^\mu \eta) + \frac{1}{2}(\partial_\mu \xi)(\partial^\mu \xi) - V(\eta, \xi), \tag{3.13}$$

where the potential $V(\eta, \xi) = \mu^2\phi^2 + \lambda\phi^4$ can be expressed as in terms of the fields η, ξ and using relation $\mu^2 = -\lambda v^2$

$$\begin{aligned} V(\eta, \xi) &= \mu^2\phi^2 + \lambda\phi^4 \\ &= -\frac{1}{2}\lambda v^2 \left[(v+\eta)^2 + \xi^2\right] + \frac{1}{4}\lambda \left[(v+\eta)^2 + \xi^2\right]^2 \\ &= -\frac{1}{4}\lambda v^4 + \lambda v^2\eta^2 + \lambda v\eta^3 + \frac{1}{4}\lambda\eta^4 + \frac{1}{4}\lambda\xi^4 + \lambda v\eta\xi^2 + \frac{1}{2}\lambda\eta^2\xi^2. \end{aligned} \tag{3.14}$$

By looking at the potential, we can identify the mass in the term quadratic in field η. The mass of the field is simply then $m_\eta = \sqrt{2\lambda v^2}$. The mass term for the field η can then be extracted and we are left with the kinetic terms, mass term and interaction potential V_{int} of Lagrangian which describes interaction between fields. The Lagrangian then reads

$$\frac{1}{2}(\partial_\mu \eta)(\partial^\mu \eta) - \frac{1}{2}m_\eta^2\eta^2 + \frac{1}{2}(\partial_\mu \xi)(\partial^\mu \xi) - V_{int}(\eta, \xi), \tag{3.15}$$

where the interaction potential is

$$V_{int}(\eta, \xi) = \lambda v\eta^3 + \frac{1}{4}\lambda\eta^4 + \frac{1}{4}\lambda\xi^4 + \lambda v\eta\xi^2 + \frac{1}{2}\lambda\eta^2\xi^2. \tag{3.16}$$

The Lagrangian in (3.15) represents field η with the mass $m_\eta = \sqrt{2\lambda v^2}$ and massless scalar field ξ, which gives rise to massless scalar particles, Goldstone bosons.

3.3 The Higgs boson

Now that we have considered real and complex scalar fields, we move towards the Higgs mechanism in the Standard Model, which is responsible for giving masses to the particles. In this section we first extend the discussion of the complex scalar field to the SSB in the presence of a local gauge symmetry $U(1)$. In the local gauge symmetry the symmetry group depends on also the spatial coordinates. This means that the field $\phi(x)$ needs to be invariant in the local gauge transformation [23]

$$\phi(x) \to \phi(x)' = e^{ig\alpha(x)}\phi. \tag{3.17}$$

The complex scalar potential remains the same as in previous section but Lagrangian changes as

$$\mathcal{L} = (D_\mu\phi)(D^\mu\phi)^* - \frac{1}{4}F_{\mu\nu}F^{\mu\nu} - V(\phi\phi^*), \tag{3.18}$$

where

$$D_\mu\phi(x) = \partial_\mu\phi(x) + igB_\mu\phi(x), \quad D_\mu\phi(x)^* = \partial_\mu\phi(x)^* - igB_\mu\phi(x)^* \tag{3.19}$$

and

$$V(\phi\phi^*) = \mu^2\phi\phi^* + \lambda(\phi\phi^*)^2, \quad F_{\mu\nu} = \partial_\mu B_\nu - \partial_\nu B_\mu, \quad B'_\mu = B_\mu - \partial_\mu\alpha. \tag{3.20}$$

By calculating the kinetic term, the whole expression of the Lagrangian becomes

$$\begin{aligned}\mathcal{L} = &-\frac{1}{4}F_{\mu\nu}F^{\mu\nu} + (\partial_\mu\phi)(\partial^\mu\phi)^* - \mu^2\phi\phi^* - \lambda(\phi\phi^*)^2 \\ &- igB_\mu\phi^*(\partial^\mu\phi) + ig(\partial_\mu\phi^*)B^\mu\phi + g^2B_\mu B^\mu\phi^*\phi.\end{aligned} \tag{3.21}$$

Now we use again a shifted vacuum state and noting that physical vacuum is chosen to be $\phi_1 + i\phi_2 = v$, the field ϕ becomes

$$\phi(x) = \frac{1}{\sqrt{2}}[(v + \eta) + i\xi] \tag{3.22}$$

and the Lagrangian has familiar form

$$\mathcal{L} = \underbrace{\frac{1}{2}(\partial_\mu \eta)^2 - \lambda v^2 \eta^2}_{\text{massive } \eta} + \underbrace{\frac{1}{2}(\partial_\mu \xi)^2}_{\text{massless } \xi} - \underbrace{\frac{1}{4}F_{\mu\nu}F^{\mu\nu} + \frac{1}{2}g^2 v^2 B_\mu B^\mu}_{\text{massive gauge field}} + gvB_\mu(\partial^\mu \xi) - V_{int}, \quad (3.23)$$

where V_{int} contains three- and four-point interactions of fields η, ξ and B_μ. By looking at the Lagrangian, we can see it is similar to Lagrangian in (3.15). This newly obtained form has one term which is hard to interpret, namely $gvB_\mu(\partial^\mu \xi)$. By using freedom to redefine the field B_μ to clear up the terms that involve the massless field ξ. Then we have [24]

$$\frac{1}{2}(\partial_\mu \xi)^2 + gvB_\mu(\partial^\mu \xi) + \frac{1}{2}g^2 v^2 B_\mu^2 = \frac{1}{2}g^2 v^2 \left(B_\mu + \frac{1}{gv}(\partial_\mu \xi)\right)^2 = \frac{1}{2}g^2 v^2 (B'_\mu)^2, \quad (3.24)$$

where we have chosen $\alpha = -\xi/gv$. This choice is called a *unitary gauge* and it changes the field ϕ accordingly. Now we may perform the local gauge transformation with the unitary gauge. Transforming the field ϕ allows us to introduce new scalar field h as follows

$$\begin{aligned} \phi \to \phi' = e^{-i\xi/v}\phi = e^{-i\xi/v}\frac{1}{\sqrt{2}}(v + \eta + i\xi) \approx e^{-i\xi/v}\frac{1}{\sqrt{2}}(v+\eta)(1 + i\xi/v) \\ \approx e^{-i\xi/v}\frac{1}{\sqrt{2}}(v+\eta)e^{i\xi/v} = \frac{1}{\sqrt{2}}(v+\eta) = \frac{1}{\sqrt{2}}(v+h), \end{aligned} \quad (3.25)$$

where we have dropped higher order terms and introduced the real h-field. By using this specific gauge, we can get rid of the massless field ξ and the additional degree of freedom (DoF) comes from the broken gauge symmetry. This gives mass term for the gauge boson. The field ξ couples to the field B_μ and it has an additional DoF and therefore additional longitudinal polarization state. The SSB grants additional DoF for every broken generator which is known as the Goldstone theorem [25]. The Lagrangian in the unitary gauge is then

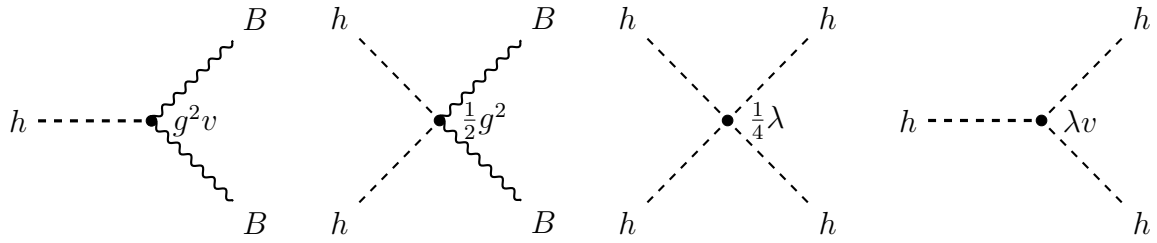

Figure 3.4: Interactions between Higgs and gauge field with Higgs field self-interactions.

$$
\begin{aligned}
\mathcal{L} &= (D_\mu\phi)(D^\mu\phi)^* - \frac{1}{4}F_{\mu\nu}F^{\mu\nu} - V(\phi^*\phi) \\
&= \frac{1}{2}(\partial_\mu + igB_\mu)(v+h)(\partial^\mu - igB^\mu)(v+h) - \frac{1}{4}F_{\mu\nu}F^{\mu\nu} - V(\phi^*\phi) \\
&= \frac{1}{2}(\partial_\mu h)(\partial^\mu h) + \frac{1}{2}g^2B_\mu B^\mu(v+h)^2 - \frac{1}{4}F_{\mu\nu}F^{\mu\nu} - \lambda v^2h^2 - \lambda vh^3 - \frac{1}{4}\lambda h^4 + \frac{1}{4}\lambda v^4 \\
&= \underbrace{\frac{1}{2}(\partial_\mu h)(\partial^\mu h) - \lambda v^2h^2}_{\text{massive scalar field}} \underbrace{- \frac{1}{4}F_{\mu\nu}F^{\mu\nu} + \frac{1}{2}g^2v^2B_\mu B^\mu}_{\text{massive gauge field}} + \underbrace{g^2vB_\mu B^\mu h + \frac{1}{2}g^2B_\mu B^\mu h^2}_{h,B\text{ interactions}} \\
&\quad \underbrace{- \lambda vh^3 - \frac{1}{4}\lambda h^4}_{h\text{ self interactions}},
\end{aligned}
\tag{3.26}
$$

where we have ignored the term $\lambda v^4/4$. The $U(1)$ local gauge theory gives rise to the interaction terms of the gauge field B_μ and the physical scalar field h. These interactions are illustrated in the Figure 3.4. The mass of the gauge boson is identified from the equation (3.15) which is

$$m_B = gv. \tag{3.27}$$

However the vacuum expectation value (vev) and the strength of the coupling of the gauge boson is directly connected to the Higgs field and Higgs boson. The mass of the Higgs boson is [16]

$$m_H = \sqrt{2\lambda}v. \tag{3.28}$$

As we can see from the expressions for masses of the bosons, the vev acts as a scale for the mass.

3.4 The Standard Model Higgs

The formulation of the Higgs mechanism in the SM differs from the section 3.3. The SM takes also into account the gauge symmetry of the electroweak interactions $SU(2)_L \times U(1)_Y$ with the gauge bosons $W_\mu^\pm, W_\mu^3$ and B_μ [26]. The Higgs sector of the SM includes Higgs doublet which is

$$\Phi = \frac{1}{\sqrt{2}} \begin{pmatrix} \phi^+ \\ \phi^0 \end{pmatrix} = \frac{1}{\sqrt{2}} \begin{pmatrix} \phi_1 + i\phi_2 \\ \phi_3 + i\phi_4 \end{pmatrix}. \tag{3.29}$$

The masses of the gauge bosons are extracted from Higgs Lagrangian that consists of Higgs potential and the kinetic term of the Higgs field. This can be written as

$$\mathcal{L}_H = |D_\mu \Phi|^2 - V(\Phi^\dagger \Phi). \tag{3.30}$$

The Higgs potential and the covariant derivative are

$$V(\Phi) = \mu^2 \Phi^\dagger \Phi + \lambda (\Phi^\dagger \Phi)^2, \tag{3.31}$$

$$D_\mu = \partial_\mu + ig\tau^a W_\mu^a + \frac{i}{2} g' Y B_\mu, \tag{3.32}$$

where $\tau^a = \frac{1}{2}\sigma^a$ are the generators of the $SU(2)$ symmetry group and hypercharge is $Y = 2(Q - I^3)$. The lower component of the Higgs doublet is neutral and has the isospin $I^3 = -\frac{1}{2}$. This leads to hypercharge to be $Y = 1$. When $\mu^2 < 0$, the potential has an infinite set of degenerate minima that satisfies the condition

$$\Phi^\dagger \Phi = \frac{1}{2}(\phi_1^2 + \phi_2^2 + \phi_3^2 + \phi_4^2). \tag{3.33}$$

When the gauge symmetry is applied, it allows us to get rid of degrees of freedom that are not physical. In this case we use unitary gauge, so we can set $\phi_1 = \phi_2 = \phi_4 = 0$ and $\phi_3 = v + h$. This modifies the Higgs doublet as follows

$$\Phi = \frac{1}{\sqrt{2}} \begin{pmatrix} 0 \\ v + h \end{pmatrix}. \tag{3.34}$$

With the definition of the covariant derivative in (3.32), we can express the kinetic term in the Lagrangian (3.30) as follows

$$\begin{aligned}|D_\mu\phi|^2 =&\frac{1}{2}(\partial_\mu h)(\partial^\mu h) + \frac{1}{8}g^2(W_\mu^1 + iW_\mu^2)(W^{(1)\mu} - iW^{(2)\mu})(v+h)^2 \\ &+ \frac{1}{8}(gW_\mu^3 - g'B_\mu)(gW^{(3)\mu} - g'B^\mu)(v+h)^2. \end{aligned} \tag{3.35}$$

The mass terms for the gauge boson fields can be extracted as quadratic in the terms of the gauge boson fields, so we obtain [27]

$$|D_\mu\phi|^2 = g^2\frac{v^2}{8}\left[(W_\mu^1)^2 + (W_\mu^2)^2 + \left(\frac{g'}{g}B_\mu - W_\mu^3\right)^2\right]. \tag{3.36}$$

The mass terms for the gauge fields W_μ^1 and W_μ^2 can be identified as

$$\frac{1}{2}m_W^2 W_\mu^1 W^{(1)\mu} \quad \text{and} \quad \frac{1}{2}m_W^2 W_\mu^2 W^{(2)\mu}, \tag{3.37}$$

with the mass of the W boson to be

$$m_W = \frac{1}{2}gv. \tag{3.38}$$

The expression of (3.36) tells us that there exists three massive gauge bosons. The kinetic terms for the gauge fields B_μ and W_μ^a are canonically normalized and diagonalizing the masses by defining

$$\begin{cases} Z_\mu \equiv \cos\,\theta_w W_\mu^3 - \sin\,\theta_w B_\mu \\ A_\mu \equiv \sin\,\theta_w W_\mu^3 + \cos\,\theta_w B_\mu \end{cases} \Leftrightarrow \quad \begin{cases} B_\mu = \cos\,\theta_w A_\mu - \sin\,\theta_w Z_\mu \\ W_\mu^3 = \sin\,\theta_w A_\mu + \cos\,\theta_w Z_\mu, \end{cases} \tag{3.39}$$

with

$$\tan\,\theta_w = \frac{g'}{g}, \tag{3.40}$$

where θ_w is the Weinberg angle. This angle is defined with the coupling constants g

and g' as follows [18]

$$\sin\,\theta_w = \frac{g'}{\sqrt{g^2+g'^2}}, \qquad \cos\,\theta_w = \frac{g}{\sqrt{g^2+g'^2}}. \tag{3.41}$$

If we now consider the term $gW_\mu^3 - g'B_\mu$ from the Lagrangian and use the definitions from above, we obtain

$$\begin{aligned} gW_\mu^3 - g'B_\mu &= \sqrt{g^2+g'^2}\left(\frac{g}{\sqrt{g^2+g'^2}}W_\mu^3 - \frac{g'}{\sqrt{g^2+g'^2}}B_\mu\right) \\ &\equiv \sqrt{g^2+g'^2}\left(\cos\,\theta_w W_\mu^3 - \sin\,\theta_w B_\mu\right) \\ &\equiv \sqrt{g^2+g'^2}Z_\mu. \end{aligned} \tag{3.42}$$

The mass for the Z boson is acquired from the Lagrangian (3.35) by identifying the mass term,

$$\begin{aligned} \mathcal{L} &\sim \frac{1}{8}(v+h)^2(gW_\mu^3 - g'B_\mu)^2 \\ &= \frac{1}{8}(g^2+g'^2)(v+h)^2 Z_\mu Z^\mu \\ &= \frac{1}{8}(g^2+g'^2)v^2 Z_\mu Z^\mu + \frac{1}{4}(g^2+g'^2)vhZ_\mu Z^\mu + \frac{1}{8}(g^2+g'^2)hhZ_\mu Z^\mu, \end{aligned} \tag{3.43}$$

where the mass of the Z boson is

$$m_Z = \frac{v}{2}\sqrt{g^2+g'^2} = \frac{gv}{2\cos\,\theta_w} = \frac{m_W}{\cos\,\theta_w}. \tag{3.44}$$

With similar procedure, the gauge field A_μ can be interpreted as a massless neutral gauge boson, photon and represented as

$$A_\mu = \frac{g'W_\mu^3 + gB_\mu}{\sqrt{g^2+g'^2}} \quad \text{with} \quad m_A = 0. \tag{3.45}$$

The SM Higgs model is described with four parameters with electroweak symmetry breaking. Two of these parameters come from Higgs potential λ, μ and two from the gauge couplings g' and g of the group $SU(2)_L \times U(1)_Y$. The mass of

the Higgs boson and the vev of the Higgs field are represented with these parameters as

$$v^2 = -\frac{\mu^2}{\lambda} \quad \text{and} \quad m_H^2 = 2\lambda v^2. \tag{3.46}$$

By using measured values for the coupling constant g and the mass of the W boson as well as relation $m_W = \frac{1}{2}gv$, we find that the vacuum expectation value of the Higgs field is

$$v = 246 \text{ GeV}. \tag{3.47}$$

This is a remarkable result since it sets electroweak scale for the interactions that contain gauge bosons.

Chapter 4

Properties of the Higgs boson

The Higgs boson was discovered at the Large Hadron Collider (LHC) from CMS and ATLAS experiments [8], [28]. In the CMS experiment Higgs boson was discovered through proton-proton collisions at the centre-of-mass energy being $\sqrt{s} = 7$ TeV. The search of the Higgs was focused on five decay modes: $\gamma\gamma, ZZ, W^+W^-, \tau^+\tau^-$ and $\bar{b}b$. The two main decay modes with best mass resolution are $\gamma\gamma$ and ZZ, which indicate that mass of the Higgs boson is around 125 GeV. The ATLAS experiment searches Higgs boson where it produces a resonant mass peak in the decay channels $H \to ZZ \to 4\ell$, $H \to WW \to \ell\nu\ell\nu$ and $H \to \gamma\gamma$.

4.1 Production of the Higgs

In proton-proton collisions the Higgs production occurs via gluon fusion (ggF) and vector boson fusion (VBF), where V refers to W or Z gauge bosons. These are main production mechanisms for the Higgs boson. Gluon fusion production mechanism is dominated by top-quarks (ttH diagram). The lowest order Feynman diagram for the Higgs production with ggF is shown in the Figure 4.1. Higgs production from the gauge bosons W and Z is illustrated in the Figure 4.2.

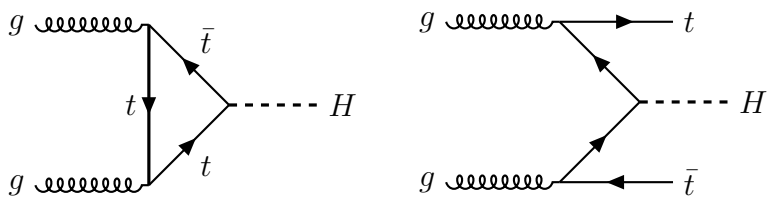

Figure 4.1: Higgs production via gluon fusion.

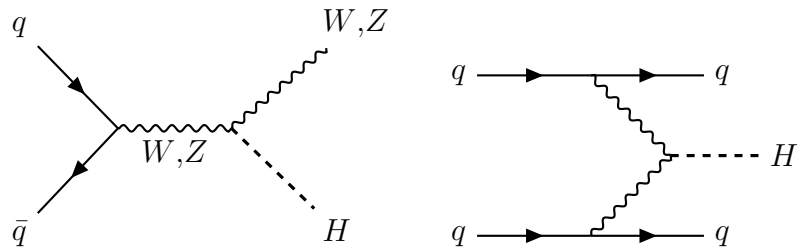

Figure 4.2: Higgs production via Higgsstrahlung and vector boson fusion.

Regarding the Higgs production, the ggF, $gg \to H$ + jets has the largest cross section respect to other production processes [29]. The ggF process occurs through a loop diagram which is dominated by the top quark as indicated in the Figure 4.1. The loops that contain lighter quarks, other than the top quark, are suppressed by the factor which is proportional to m_q^2, where m_q is the mass of the quark. This means that it is good to assume that Higgs is produced via top quark loop in ggF for qqH coupling. Since we are dealing with the gluons, the QCD radiative corrections must be taken account. The ggF cross section has been measured very precisely at the next-to-leading order (NLO) and the next-to-next-to-leading order (NNLO). These terms can be compared to the perturbative expansion in strong coupling constant α_s in QCD. The NLO corrections of the QCD improve the leading-order (LO) prediction by 80%. In addition, the NLO increases the prediction by 20%. For the Higgs boson mass $m_H \approx 125$ GeV, there is also NLO corrections for the electroweak sector which increase the cross section slightly, approximately 5%.

After the ggF, the next largest cross section in the Higgs boson production is due to VBF [29]. This process is illustrated in the Figure 4.2, where Higgs is produced in pp collisions, which creates W and Z bosons. Furthermore they annihilate each other to create the Higgs boson. Another channel is Higgsstrahlung, where quark and antiquark pair annihilate to create W or Z boson, which then emits the Higgs. In VBF, the scattered quarks form two hard hjets which distinguishes them from the ggF process. Similar process to VBF is production of the W and Z boson (VH) along with the Higgs. The corresponding cross section comes from the process $pp \to \mathrm{VH} + X$, where the corrections of the QCD has been computed up to NNLO and electroweak corrections up to NLO. Higgs boson radiates to top quarks in the process $pp \to Ht\bar{t}$. This channel can give an insight for Higgs decay into other quarks like b quarks when considering quark-Higgs Yukawa coupling. Total cross section is increased 20% by LO and NLO QCD corrections. In the Figure 4.3 Higgs boson production cross section is

represented in pico barns as the function of the centre-of-mass energy in pp collisions for every production channel.

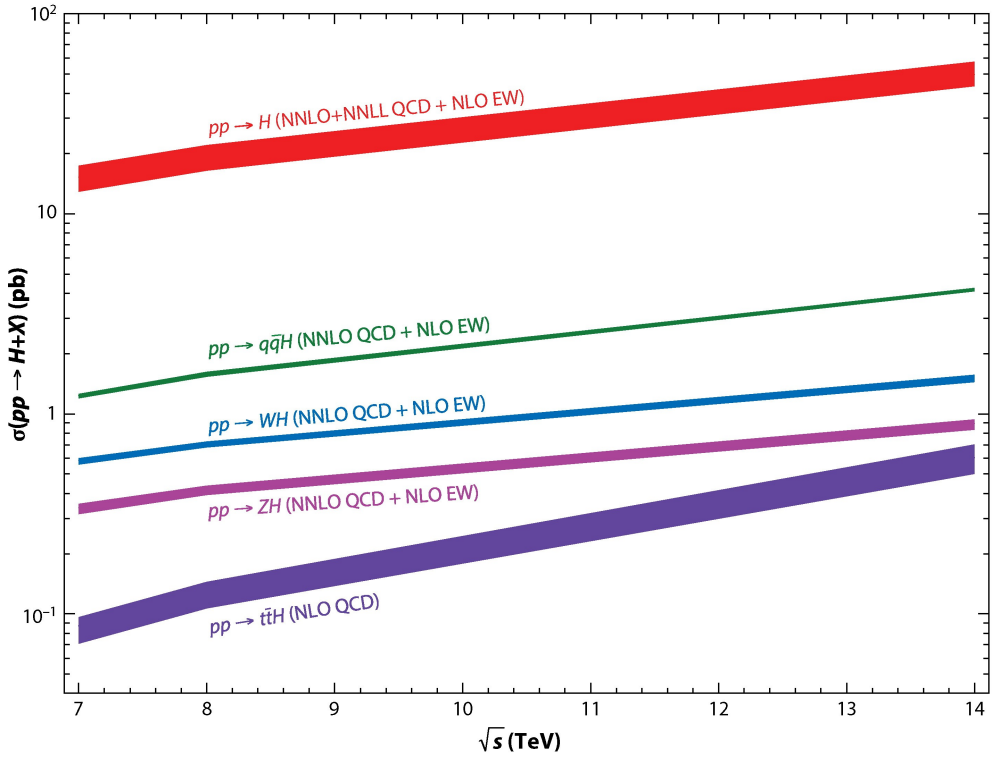

Figure 4.3: Cross sections of the SM Higgs boson production channels for $m_H = 125$ GeV [29]. The width of the bands indicate the uncertainty of the process [30].

4.2 Decay channels and measurement of the Higgs boson

Now that we know the production mechanism of the Higgs boson, we can now focus on decay channels. Since the Higgs boson is massive (125 GeV), it cannot be measured directly due to its short lifetime $\sim 10^{-22}$ s, so we need to consider its decay channels to measure its mass [31]. The first observations of the Higgs boson were made through $\gamma\gamma, ZZ$ and WW channels which were studied in the CMS experiment [8]. Other channel that could be used to measure Higgs boson mass is H$\to ZZ \to 4\ell$, which was done by the CMS [32]. The decay channels to two photons (diphoton channel) of the Higgs is illustrated in the Figure 4.4.

The mass of the Higgs boson is measured using a resonant peak in the mass $m_{\gamma\gamma}$ in diphoton channel [9]. This peak is observed from the monotonically decreasing mass

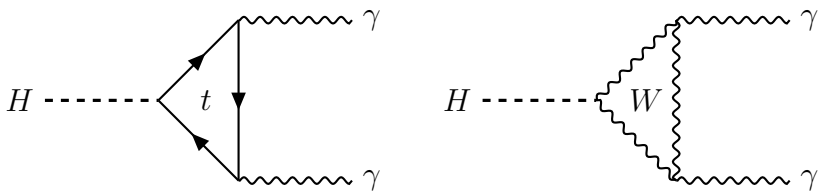

Figure 4.4: Feynman diagrams for the decay channel H $\rightarrow \gamma\gamma$.

distribution of the $m_{\gamma\gamma}$. The mass of two diphoton is calculated by using energies of two photons and relative directions respect to production vertex. Then a neural-network algorithm based on primary vertex and on track information is used to reconstruct primary vertex candidates. The events that are selected will be divided into different categories based on their signal-to-background ratios and mass resolution. Furthermore after an initial selection the events are selected by the pseudorapidity to be $|\eta| < 1.37$ or $1.52 < |\eta| < 2.37$ for the two photon candidates that are identified. The events are selected if the ratio of transverse energy respect to diphoton mass is $E_T/m_{\gamma\gamma} > 0.35$ and 0.25 respectively. These constraints allows us to limit the diphoton invariant mass to be in range 105 GeV $< m_{\gamma\gamma} <$ 160 GeV.

The peak in the diphoton mass spectrum indicates a signal of Higgs boson [33]. The distribution for the signal is determined empirically and can be modelled as a double-sided Crystal Ball function. The function consists of Gaussian peak in the distribution, where Higgs boson signal creates a peak and both sides of the Gaussian part distribution obeys power law. Regarding the mass resolution, most of the contribution for the non-Gaussian part is due to photon that is converted into an electron-positron pair $\gamma \rightarrow e^+e^-$. Diphoton invariant mass value is used to parametrize the invariant mass distribution of the background for all categories. The parameters are fitted in the data. Resulting outcome for invariant mass spectrum of the diphoton mass $m_{\gamma\gamma}$ is shown in the Figure 4.5.

Similarly to decay channel H $\rightarrow \gamma\gamma$, Higgs boson can be computed using decay channel into four leptons as H $\rightarrow ZZ \rightarrow 4\ell$ [8]. The corresponding Feynman diagram for the decay $ZZ \rightarrow 4\ell$ is shown in the Figure 4.6, where ℓ is either e or μ. Event selection takes also place in this experiment. For the selection, electrons must have at least transverse energy $p_T > 7$ GeV and pseudorapidity of $|\eta| < 2.5$. Muons on the other hand must have $p_T > 5$ GeV and $|\eta| < 2.4$ respectively. The lepton pairs of muons and electrons from Z boson decays must originate from same vertex, which indicates decay of the Higgs boson. After the decay to lepton pairs, the radiation is produced in the final state and can be used to compute lepton-pair invariant mass. Selected events for the decay channel $ZZ \rightarrow 4\ell$ fall in mass range of $110 < m_{4\ell} <$ 160 GeV, where $m_{4\ell}$ is the four-lepton invariant mass. The mass distribution of the four

leptons gives us the histogram that is shown in the Figure 4.7. It is easy to notice that there is a peak in the Z boson mass region (90 GeV) as well as smaller peak around the mass of the Higgs boson (125 GeV) where the masses are reconstructed.

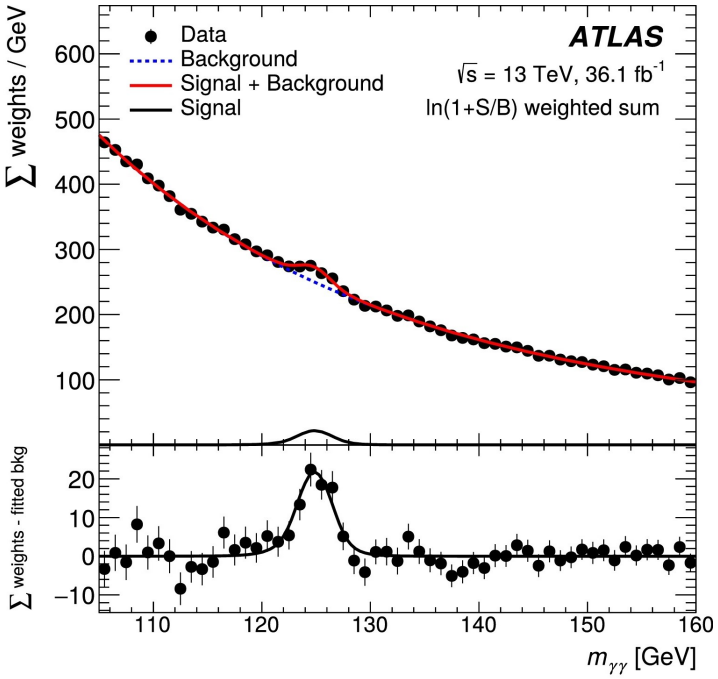

Figure 4.5: Diphoton invariant mass distribution of all selected data events with fit. Each category of data and signal are weighted by factor $\ln(1 + S/B)$, where S and B are yields of background and data in $m_{\gamma\gamma}$. The background is described by blue dotted line, signal by black line and signal + background by red line. Bottom plot shows difference background and the sum of the weights [9].

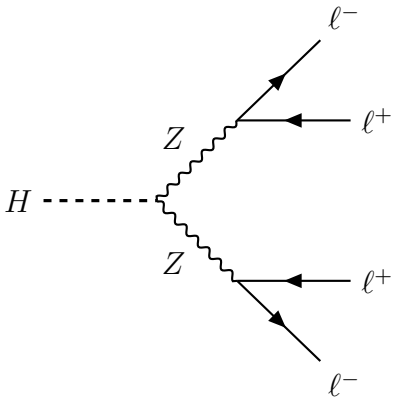

Figure 4.6: Higgs boson decay channel into four leptons H $\rightarrow ZZ \rightarrow 4\ell$ ($\ell = e, \mu$).

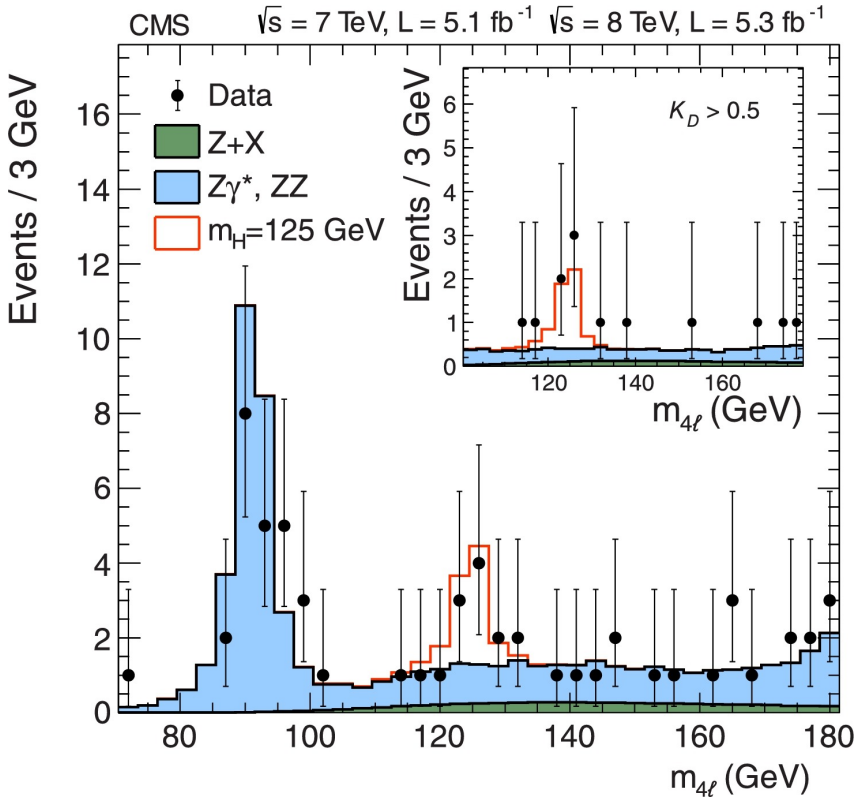

Figure 4.7: Mass distribution of the four-lepton decay channel H $\rightarrow ZZ \rightarrow 4\ell$ [8].

4.3 Branching ratios of the Higgs boson

To understand and interpret the data and measurements from the LHC, we need to calculate all decay widhts Γ_i of the Higgs boson [29]. The branching ratios of the decay channels are calculated by using ratio $\mathrm{BR}_i = \Gamma_i/\Gamma_{tot}$ for each process. From the CMS and ATLAS experiments of the LHC, the dominant decay channels of the SM Higgs boson with mass of 125 GeV are $H \rightarrow b\bar{b}$, $H \rightarrow WW$, $H \rightarrow \tau^+\tau^-$, $H \rightarrow ZZ$ and $H \rightarrow \gamma\gamma$. Some decays like $H \rightarrow \mu^-\mu^+$ and $H \rightarrow \gamma Z$ are harder to detect, since they have low decay rates and lack presence of background, which produces same particles in the final state as the main decay channels. Decay channels that contain a loop, like $H \rightarrow gg$, $H \rightarrow \gamma Z$ and $H \rightarrow \gamma\gamma$ give indirectly information about the fermionic and bosonic couplings WW, $t\bar{t}$ on Higgs boson. Branching ratios of the main decay modes are shown in the Figure 4.8 and their corresponding numerical values in the Table 4.1.

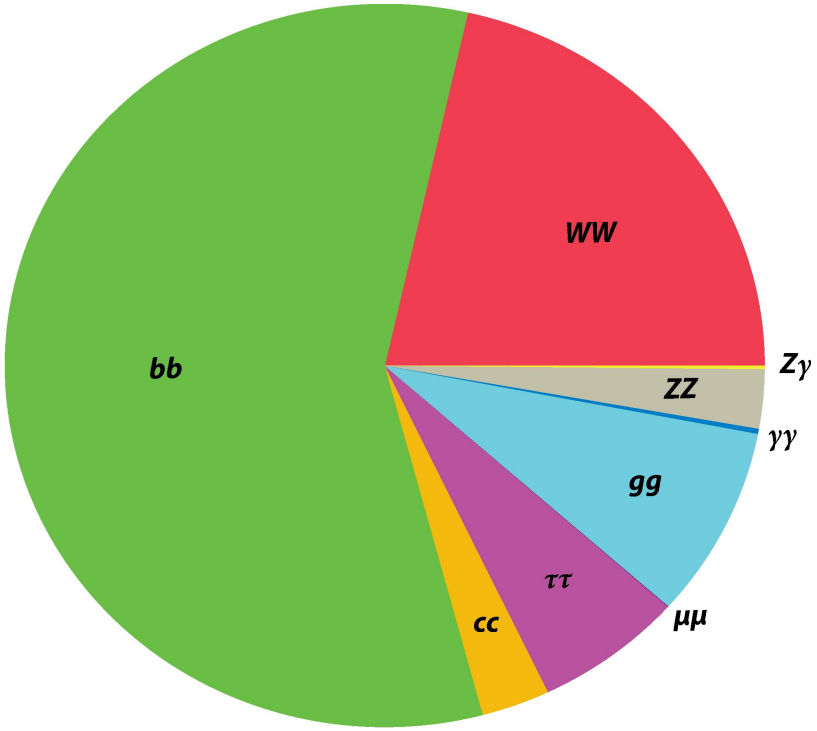

Figure 4.8: Branching ratios of the main decay channels for the SM Higgs boson with mass of $m_H = 125$ GeV [29].

Decay channel	Branching ratio
$H \to b\bar{b}$	$5.77 \cdot 10^{-1}$
$H \to WW$	$2.15 \cdot 10^{-1}$
$H \to gg$	$8.57 \cdot 10^{-2}$
$H \to \tau\tau$	$6.32 \cdot 10^{-2}$
$H \to c\bar{c}$	$2.91 \cdot 10^{-2}$
$H \to ZZ$	$2.64 \cdot 10^{-2}$
$H \to \gamma\gamma$	$2.28 \cdot 10^{-3}$
$H \to Z\gamma$	$1.54 \cdot 10^{-3}$
$H \to \mu^+\mu^-$	$2.20 \cdot 10^{-4}$

Table 4.1: Numerical values of the branching ratios for main decay modes of the SM Higgs [34].

Chapter 5

Fitting SM to LHC data

Now that we have gone through the properties of the Higgs boson, it is time to fit the obtained data from the LHC to SM. Higgs has five main production channels in proton-proton collisions, which were ggF, VBF, ttH and VH. These are illustrated in the Figures 4.1 and 4.2. Decay channels that we are focusing on are $bb, \tau\tau, ZZ, WW$ and $\gamma\gamma$. To measure the yield of the Higgs boson and its SM expectation, we need to study signal strengths of different production and decay modes [35]. For a specific production and decay channel $i \to H \to f$ the signal strengths μ_i and μ^f are defined as

$$\mu_i = \frac{\sigma_i}{(\sigma_i)_{\mathrm{SM}}} \qquad \text{and} \qquad \mu^f = \frac{\mathrm{BR}^f}{(\mathrm{BR})^f_{\mathrm{SM}}}. \tag{5.1}$$

Here σ_i (i = ggF, VBF, VH, ttH) stands for cross section of the production channel $i \to H$ and BR^f branching ratio for the decay channel $H \to f$, ($f = bb, \tau\tau, ZZ, WW, \gamma\gamma$) respectively. In the SM the signal strengths of both decay and production channels are one ($\mu_i = \mu^f = 1$). In the experiments, only the product of signal strengths can be extracted from the data because we would need to make more assumptions for the cross section and branching ratio. Then, the combined signal strength of the decay and production channel becomes

$$\mu_i^f = \frac{\sigma_i \cdot \mathrm{BR}^f}{(\sigma_i)_{\mathrm{SM}} \cdot (\mathrm{BR})^f_{\mathrm{SM}}}. \tag{5.2}$$

In this case we study how the SM Higgs boson fits the latest LHC results from CMS with the center of mass energies $\sqrt{s} = 13$ TeV. All combinations from the

Decay mode	Production process				
	ggH	VBF	WH	ZH	ttH
$H \to bb$	$2.51^{+2.44}_{-2.01}$	-	$1.73^{+0.70}_{-0.68}$	$0.99^{+0.48}_{-0.45}$	$0.91^{+0.45}_{-0.43}$
$H \to \tau\tau$	$1.05^{+0.53}_{-0.47}$	$1.12^{+0.45}_{-0.43}$	-	-	$0.22^{+1.03}_{-0.88}$
$H \to WW$	$1.35^{+0.20}_{-0.19}$	$0.28^{+0.64}_{-0.60}$	$3.91^{+2.26}_{-2.01}$	$0.96^{+1.81}_{-1.46}$	$1.60^{+0.66}_{-0.59}$
$H \to ZZ$	$1.22^{+0.24}_{-0.21}$	$-0.09^{+1.02}_{-0.76}$	$0.00^{+2.32}_{+0.00}$	$0.00^{+4.26}_{+0.00}$	$0.00^{+1.51}_{+0.00}$
$H \to \gamma\gamma$	$1.15^{+0.21}_{-0.18}$	$0.68^{+0.59}_{-0.45}$	$3.71^{+1.49}_{-1.35}$	$0.00^{+1.13}_{+0.00}$	$2.14^{+0.87}_{-0.74}$

Table 5.1: Best-fit signal strength values $\mu_i^f = \mu_i \times \mu^f$ for each given production and decay channel $i \to H \to f$. The uncertainty of each signal strength is $\pm 1\sigma$ [35].

production and decay channels are given in the Table 5.1. To study how SM Higgs fits the latest CMS results, we consider an effective Lagrangian of form which describes interactions of the desired production and decay channels [36]

$$\mathcal{L}_{eff} = a_V \frac{2m_W^2}{v_w} h W_\mu^+ W^{-\mu} + a_V \frac{m_Z^2}{v_w} Z_\mu Z^\mu - a_f \sum_{\psi=t,b,\tau} \frac{m_\psi}{v_w} h \bar{\psi}\psi, \tag{5.3}$$

where interaction terms for bosons are multiplied by a_V and fermions by a_f. Third term has a colour singlet scalar and a vector boson. Mass parameters are fixed to the physical masses of the corresponding particles and v_w stands for the electroweak (EW) vacuum expectation value, $v_w = 246$ GeV. One may notice that if we set $a_V = a_f = 1$, we have interaction terms of the SM. Since the combined signal strength depends on the cross section and branching ratio as defined in the equation (5.2), we can write them separately in terms of the coupling coefficients a_V and a_f in equation (5.1). Therefore we have for the production channels [36],

$$\mu_{VBF} = \mu_{WH} = \mu_{ZH} = |a_V|^2, \qquad \mu_{ttH} = \mu_{ggF} = |a_f|^2 \tag{5.4}$$

and

$$\mu^{bb} = \mu^{\tau\tau} = |a_f|^2, \qquad \mu^{ZZ} = \mu^{WW} = |a_V|^2 \tag{5.5}$$

respectively for decay channels.

The diphoton decay channel $H \to \gamma\gamma$ appears to be a little problematic since it has both fermionic and bosonic decay channels as illustrated by Feynman diagrams

in the Figure 4.4. It has a top quark and W boson loop of the same order. Now we need to compute its amplitude as the function of a_V and a_f. By using the analytical formula given in [37], we write

$$\Gamma_{\gamma\gamma}(a_f, a_V) = \frac{G_F \alpha^2 m_h^3}{128\sqrt{2}\pi^3} |a_V F_1(\tau_W) + a_f N_c Q_t^2 F_{1/2}(\tau_t)|^2, \tag{5.6}$$

where $N_c = 3$ is the number of colours, G_F is the Fermi constant, Q_t is the electric charge of the top quark and $\tau_j = 4m_j^2/m_h^2$, $i = W, t$. Previous equation can further simplified as

$$\Gamma_{\gamma\gamma}(a_f, a_V) = \frac{\alpha^2 g^2 m_h^3}{1024 m_W^2 \pi^3} |a_V F_1(\tau_W) + \frac{4}{3} a_f F_{1/2}(\tau_t)|^2, \tag{5.7}$$

where [38]

$$F_{1/2} = -2\frac{4m_t^2}{m_h^2}\left(1 + \left(1 - \frac{4m_t^2}{m_h^2}\right) f\left(\frac{4m_t^2}{m_h^2}\right)\right), \tag{5.8}$$

$$F_1 = 2 + 3\frac{4m_W^2}{m_h^2} + 3\frac{4m_W^2}{m_h^2}\left(2 - \frac{4m_W^2}{m_h^2}\right) f\left(\frac{4m_W^2}{m_h^2}\right) \tag{5.9}$$

and

$$f(\tau) = \begin{cases} \arcsin^2 \sqrt{\frac{1}{\tau}}, & \tau \geq 1, \\ -\frac{1}{4}\left[\log\left(\frac{\sqrt{1-\tau}+1}{1-\sqrt{1-\tau}}\right) - i\pi\right]^2, & \tau < 1. \end{cases} \tag{5.10}$$

Using numerical values for the constants $m_W = 80.4$ GeV, $m_h = 125$ GeV, $\alpha = 1/137$ (fine structure constant) and $g = 0.653$ yields the signal strength for the decay

$$\mu^{\gamma\gamma} = \frac{\Gamma_{\gamma\gamma}}{\Gamma_{\gamma\gamma}(a_V = 1, a_f = 1)} \approx 0.024\,(1.83 a_f - 8.32 a_V)^2\,. \tag{5.11}$$

Now we use the signal strength values from the Table 5.1 to calculate signal strength values for $\mu_{exp}(a_f, a_V)$ as the function of the parameters a_V and a_f from the

Lagrangian (5.3). To obtain the best fit values for the both parameters, we use the method of least squares which is further described in Appendix A. The idea of the method is to minimize χ^2 function with the respect of a_V and a_f. Then the function that needs to minimized is [39]

$$\chi^2(a_f, a_V) = \sum \left(\frac{\mu_{exp} - \mu_{obs}}{\delta\mu_{obs}} \right)^2 , \tag{5.12}$$

where μ_{obs} is the observed signal strength and $\delta\mu_{obs}$ is its error. Due to signal strengths $\mu_i = \mu^f = 1$ in the SM, it is reasonable to expect that the parameters a_V and a_f are close to one. After the minimization, we calculate the $1\sigma, 2\sigma$ and 3σ confidence level (CL) regions by using formula $\chi^2 = \chi^2_{min} + \delta_n$ [40]. Here δ_n denotes the values of $\Delta\chi$ for two parameters. The corresponding values for the CL regions $1\sigma = 68\%, 2\sigma = 95\%$ and $3\sigma = 99.7\%$ are $\delta_1 = 2.30, \delta_2 = 6.18$ and $\delta_3 = 11.83$. These CL regions form contours in the (a_V, a_f) -plane. This is illustrated in the Figure 5.1. Compared to the prediction of the SM $(a_V, a_f) = (1, 1)$, the best fit is really close to it $(a_V, a_f) = (0.97, 1.04)$.

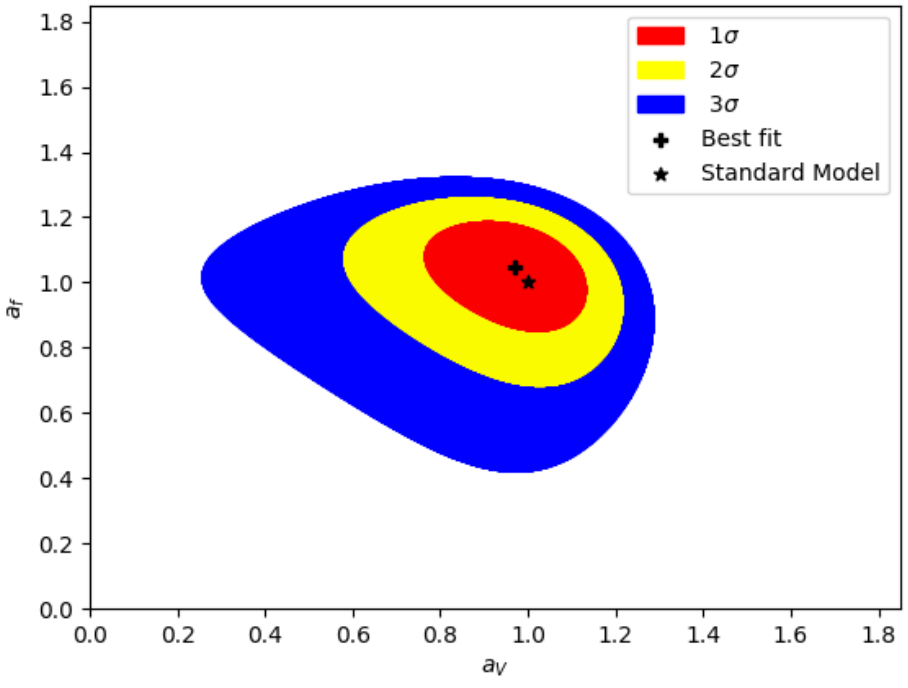

Figure 5.1: Two parameter fit for a_V and a_f. The red, yellow and blue regions correspond $1\sigma, 2\sigma$ and 3σ CL regions. The best fit for the parameters is marked by plus sign and SM prediction by a star.

Chapter 6

Conclusions and outlook

In this thesis we took a general overview of the Standard Model like its particle content and interactions, which are electromagnetic, strong and weak interaction. Gravity is not included. In the end of first chapter was noticed that the electroweak unification combines electromagnetic and weak interaction into one, electroweak interaction.

Then we moved to Higgs mechanism and discussed its main principles and how particles acquire mass through the spontaneous symmetry breaking which is a crucial phenomenon. SSB can occur for the global and local gauge symmetry from which in both cases have different but similar outcomes. SSB of the global symmetry creates massless Goldstone bosons where as the breaking of local gauge symmetry induces massive gauge fields. SM Higgs is based on the electroweak symmetry breaking that creates Goldstone bosons which give longitudinal degree of freedom. This leads to masses of $W^{\pm}$ and Z bosons.

After the in depth look into Higgs mechanism, we went through the properties of the Higgs boson like its lifetime, production, decay channels and how it is detected in the first place at the LHC. In proton-proton collisions the Higgs can be produced via gluon fusion (ggF), vector boson fusion (VBF) or Higgsstrahlung. Due to its short lifetime Higgs boson cannot be measured directly. In the ATLAS and CMS experiments, very specific decay channels were chosen to investigate the decay of the Higgs to determine its mass which turns out to be around 125 GeV. In the CMS experiment decay channel $H \to ZZ \to 4\ell$ and in ATLAS $H \to \gamma\gamma$.

Finally we fitted SM to LHC data by examining the signal strengths for the production and decay channels μ_i and μ^f, then carried data analysis for the combined signal strength μ_i^f. Every signal strength could be written in terms of coupling coefficient of the effective Lagrangian. Diphoton decay channel involved more analyzing due to W boson and top quark loops. Minimization of the χ^2 function yielded the best fit for the parameters a_V and a_f. After that $1\sigma, 2\sigma$ and 3σ confidence level region could be

extracted and form contours in the (a_V, a_f) -plane. The contours give us information about how well SM predictions correspond to LHC data. The best fit was really close the SM estimation.

Even though the accurate results of the SM, especially masses of the gauge bosons, there is still open questions which SM cannot give explanation. For instance, the hierarchy problem where there is an enormous difference between the Planck mass and the gauge boson masses. Other big problems are the dark matter, neutrino masses and baryon asymmetry which indicates an extra source of CP-violation. Hence SM is not a complete theory so it needs extensions. One way to extend SM is to make extensions to the Higgs sector. Possible extensions are two-Higgs-doublet models, triplet models and Higgs portal models which may also provide for dark matter candidates. These models are further described in [41, 42, 43]. Also implementing supersymmetry into SM with minimal supersymmetric SM (MSSM) is discussed in [44].

The methodology developed in this thesis for the analysis of the Standard Model can be extended to similarly analyse and constrain various beyond the Standard Model scenarios with extended scalar sectors.

Appendix A

Statistics

This is summary and theory of the statistics in the data analysis in Chapter 5. Complete review can be seen in the reference [40].

Suppose that we have likelihood $L(\boldsymbol{\theta}) = P(\boldsymbol{x}|\boldsymbol{\theta})$ and set of measured quantities $\boldsymbol{x}$ for a set of parameters $\boldsymbol{\theta} = (\theta_1, \ldots, \theta_N)$. Values of $\boldsymbol{\theta}$ that give maximum L are defined as maximum likelihood (ML) estimators. Using the properties of logarithm, it is easier to work to solve values of $\boldsymbol{\theta}$ to maximize L. It is that we need to solve likelihood equations

$$\frac{\partial L_i}{\partial \theta_i} = 0, \qquad i = 1, \ldots, N. \tag{A.1}$$

Generally likelihood can be written as product of n statistically independent quantities $\boldsymbol{x} = (x_1, \ldots, x_n)$, where each component of $\boldsymbol{x}$ follows certain probability distribution function (PDF) $f(x; \boldsymbol{\theta})$. Hence the product is

$$L(\boldsymbol{\theta}) = \prod_{i=1}^{n} f(x_i; \boldsymbol{\theta}). \tag{A.2}$$

The Gaussian distribution

$$f_G(x) = \frac{1}{\sqrt{2\pi}\sigma} e^{-\frac{(x-\mu)^2}{2\sigma^2}}, \tag{A.3}$$

then obtains the form

$$L(\boldsymbol{\theta}) = \prod_{i=1}^{n} \frac{1}{\sqrt{2\pi}\sigma_i} e^{-\frac{(x_i-\mu_i)^2}{2\sigma_i^2}}. \tag{A.4}$$

The method of the least squares (LS), which is used in this thesis, coincides with the maximum likelihood. By considering a set of n measurements with known points x_i and values for measurements y_i that are distributed as Gaussian PDF with mean $\mu(x_i;\boldsymbol{\theta})$. The variance σ^2 is assumed to be known. The logarithm of the likelihood function contains the sum of the squares

$$\chi^2(\boldsymbol{\theta}) = -2\ln L(\boldsymbol{\theta}) + \text{constant} = \sum_{i=1}^{n} \frac{(y_i - \mu(x_i;\boldsymbol{\theta}))^2}{\sigma_i^2}. \tag{A.5}$$

We note that by maximizing L, values of the parameters are same that if we minimize the function $\chi^2(\boldsymbol{\theta})$.

Constructing confidence intervals is performed when the data consists of one random variable x which follows Gaussian PDF. If there is more than one variable, the multivariate Gaussian is used. Considering simplest case, where variance σ^2 is known and the measured value x falls in the range $[\mu-\delta, \mu+\delta]$. The probability is

$$1 - \alpha = \frac{1}{\sqrt{2\pi}\sigma} \int_{\mu-\delta}^{\mu+\delta} e^{-\frac{(x-\mu)^2}{\sigma^2}} = \text{erf}\left(\frac{\delta}{\sqrt{2}\sigma}\right), \tag{A.6}$$

where erf is the Gaussian error function. For a specific choice of δ, we can construct confidence intervals. Choosing $\delta = \sigma$ gives $\alpha - 1 = 68.27\%$ if σ is known. This interval is known as a standard error. Using the different values of δ we can construct the Table A.1 which contains frequently used values for α.

α	δ	α	δ
0.3172	1σ	0.2	1.28σ
$4.55{\cdot}10^{-2}$	2σ	0.1	1.64σ
$2.7{\cdot}10^{-3}$	3σ	0.05	1.96σ
$6.3{\cdot}10^{-5}$	4σ	0.01	2.58σ
$5.7{\cdot}10^{-7}$	5σ	0.001	3.29σ
$2.05{\cdot}10^{-9}$	6σ	10^{-4}	3.29σ

Table A.1: Area of the tails α outside of the interval $[\mu - \delta, \mu + \delta]$ for Gaussian distribution.

In the particle physics experiments we are interested 5σ or higher confidence level regions when searching new particles. This is due to the fact that we are convinced that the results are not influenced with statistical errors or fluctuations of the background.

When the parameters that maximize $L(\boldsymbol{\theta})$ or minimize $\chi^2(\boldsymbol{\theta})$, one finds contours with constant $\ln L$ or χ^2. This means that confidence level regions are determined by

$$\ln L(\boldsymbol{\theta}) \geq \ln L_{max} - \Delta \ln L, \tag{A.7}$$

or for the χ^2 case

$$\chi^2(\boldsymbol{\theta}) \leq \chi^2_{min} + \Delta\chi^2. \tag{A.8}$$

When there's several parameters, the value for $2\Delta \ln L$ or $\Delta\chi^2$ changes according to the number of the parameters involved. In the Table A.2 coverage probability $1-\alpha$ is represented with different number of parameters.

$(1-\alpha)\%$	$m=1$	$m=2$	$m=3$
68.27	1.00	2.30	3.53
95.45	4.00	6.18	8.03
99.73	9.00	11.83	14.16

Table A.2: Values of $\Delta\chi^2$ or $2\Delta \ln L$ which correspond to coverage probability $1-\alpha$ for different number of parameter m.

Bibliography

[1] G. Arnison et al. Experimental observation of isolated large transverse energy electrons with associated missing energy at s=540 GeV. *Physics Letters B*, 122(1):103 – 116, 1983.

[2] G. Arnison et al. Experimental Observation of Lepton Pairs of Invariant Mass Around 95-GeV/c^2 at the CERN SPS Collider. *Phys. Lett. B*, 126:398–410, 1983.

[3] J. J. Aubert, U. Becker, P. J. Biggs, J. Burger, M. Chen, G. Everhart, P. Goldhagen, J. Leong, T. McCorriston, T. G. Rhoades, M. Rohde, Samuel C. C. Ting, Sau Lan Wu, and Y. Y. Lee. Experimental observation of a heavy particle J. *Phys. Rev. Lett.*, 33:1404–1406, Dec 1974.

[4] S. W. Herb, D. C. Hom, L. M. Lederman, J. C. Sens, H. D. Snyder, J. K. Yoh, J. A. Appel, B. C. Brown, C. N. Brown, W. R. Innes, K. Ueno, T. Yamanouchi, A. S. Ito, H. Jöstlein, D. M. Kaplan, and R. D. Kephart. Observation of a Dimuon Resonance at 9.5 GeV in 400-GeV Proton-Nucleus Collisions. *Phys. Rev. Lett.*, 39:252–255, Aug 1977.

[5] F. et al. Abe. Observation of Top Quark Production in $\overline{p}p$ Collisions with the Collider Detector at Fermilab. *Phys. Rev. Lett.*, 74:2626–2631, Apr 1995.

[6] Peter W. Higgs. Broken Symmetries and the Masses of Gauge Bosons. *Phys. Rev. Lett.*, 13:508–509, Oct 1964. [Online; accessed 11-12-2019].

[7] The ATLAS Collaboration. Observation of a new particle in the search for the Standard Model Higgs boson with the ATLAS detector at the LHC, 2012.

[8] Observation of a new boson at a mass of 125 GeV with the CMS experiment at the LHC. *Physics Letters B*, 716(1):30 – 61, 2012.

[9] M. Aaboud et al. Measurement of the Higgs boson mass in the H $\rightarrow ZZ \rightarrow 4l$ and H $\rightarrow \gamma\gamma$ channels with s=13 TeV pp collisions using the ATLAS detector. *Physics Letters B*, 784:345 – 366, 2018.

[10] CERN. The Standard Model. https://home.cern/science/physics/standard-model. [Online; accessed 22-11-2019].

[11] Quantum diaries. The Standard Model: a beautiful but flawed theory. https://www.quantumdiaries.org/2014/03/14/the-standard-model-a-beautiful-but-flawed-theory/. [Online; accessed 22-11-2019].

[12] Paul Dirac. The quantum theory of the emission and absorption of radiation. 1927.

[13] Richard Feynman. *The Strange Theory of light and Matter*. 1985.

[14] Julian Schwinger. On Quantum-Electrodynamics and the Magnetic Moment of the Electron. 1947.

[15] The Search for the Graviton. https://blog.thingswedontknow.com/2016/08/search-for-the-graviton.html. [Online; accessed 24-11-2019].

[16] Mark Thomson. *Modern Particle Physics*. Cambridge University Press, 2013.

[17] Christopher G. Tully. *Elementary particle physics in a nutshell*. 2011.

[18] W. Buchmüller and C. Lüdeling. Field Theory and Standard Model, 2006.

[19] A. Pich. The Standard Model of Electroweak Interactions, 2005.

[20] Jens Erler and Shufang Su. The weak neutral current, Jul 2013.

[21] V. A. Bednyakov, N. D. Giokaris, and A. V. Bednyakov. On Higgs mass generation mechanism in the Standard Model, 2007.

[22] Spontaneous symmetry breaking in gauge theories. https://http://inspirehep.net/record/1637087/files/fulltext.pdf. [Online; accessed 20-12-2019].

[23] Higgs Mechanism. http://bolvan.ph.utexas.edu/~vadim/Classes/2019f/Higgs.pdf. [Online; accessed 13-01-2020].

[24] Ivo van Vulpen. The Standard Model Higgs Boson. http://web.mst.edu/~hale/courses/Physics_357_457/Notes/Lecture.17.Higgs.Mechanism/HiggsLectureNote.pdf, 2013-2014. [Online; accessed 04-02-2020].

[25] J Goldstone. Field theories with "superconductor" solutions. *Nuovo Cimento*, 19(CERN-TH-118):154–164, Aug 1960.

[26] L. Díaz Cruz. The Higgs profile in the Standard Model and beyond. *Revista Mexicana de Fisica*, 65(5 Sept-Oct):419, Sep 2019.

[27] Matthew D. Schwartz. *Quantum Field Theory and the Standard Model*. Cambridge University Press, 3 2014.

[28] Observation of a new particle in the search for the Standard Model Higgs boson with the ATLAS detector at the LHC. *Physics Letters B*, 716(1):1 – 29, 2012.

[29] William Murray and Vivek Sharma. Properties of the Higgs Boson Discovered at the Large Hadron Collider. *Annual Review of Nuclear and Particle Science*, 65(1):515–554, 2015.

[30] LHC Higgs Cross Section Working Group. Handbook of LHC Higgs Cross Sections: 1. Inclusive Observables, 2011.

[31] Evidence for the direct decay of the 125 GeV Higgs boson to fermions. *Nature Phys*, 10:557 – 560, 2014.

[32] A. M. Sirunyan, A. Tumasyan, W. Adam, F. Ambrogi, E. Asilar, T. Bergauer, J. Brandstetter, E. Brondolin, M. Dragicevic, and et al. Measurements of properties of the Higgs boson decaying into the four-lepton final state in pp collisions at s = 13 $\sqrt{s} = 13$ tev. *Journal of High Energy Physics*, 2017(11), Nov 2017.

[33] ATLAS Collaboration. Measurements of Higgs boson properties in the diphoton decay channel with 36 fb^{-1} of *pp* collision data at $\sqrt{s} = 13$ TeV with the ATLAS detector, 2018.

[34] LHC Higgs Cross Section Working Group. Handbook of LHC Higgs Cross Sections: 2. Differential Distributions, 2012.

[35] Combined measurements of the Higgs boson's couplings at $\sqrt{s} = 13$ TeV. Technical Report CMS-PAS-HIG-17-031, CERN, Geneva, 2018.

[36] Tommi Alanne, Stefano Di Chiara, and Kimmo Tuominen. LHC data and aspects of new physics. *Journal of High Energy Physics*, 2014(1), Jan 2014.

[37] Marcela Carena, Ian Low, and Carlos E. M. Wagner. Implications of a modified Higgs to diphoton decay width. *Journal of High Energy Physics*, 2012(8), Aug 2012.

[38] John F. Gunion, Howard E. Haber, Gordon L. Kane, and Sally Dawson. *The Higgs Hunter's Guide*, volume 80. 2000.

[39] Vaskonen V. Extensions of the Standard Model Scalar Sector and Constraints From Colliders and Cosmology, 2013.

[40] Particle Data Group. Review of Particle Physics. *Progress of Theoretical and Experimental Physics*, 2020(8), 08 2020. 083C01.

[41] G. C. Branco, P. M. Ferreira, L. Lavoura, M. N. Rebelo, Marc Sher, and Joao P. Silva. Theory and phenomenology of two-Higgs-doublet models, 2011.

[42] Sylvain Blunier, Giovanna Cottin, Marco A. Diaz, and Benjamin Koch. Phenomenology of a Higgs triplet model at future electron-positron colliders. *Physical Review D*, 95(7), Apr 2017.

[43] Giorgio Arcadi, Abdelhak Djouadi, and Martti Raidal. Dark Matter through the Higgs portal, 2019.

[44] Ian J R Aitchison. Supersymmetry and the MSSM: An Elementary Introduction, 2005.